Chapter 17
Fundamentals and Applications of Microsphere Resonator Circuits

Vasily N. Astratov

Abstract Dielectric microspheres, with sizes on the order of several wavelengths, support high-quality whispering gallery (WG) modes and provide nonresonant focusing of light into tiny spots termed nanoscale photonic jets. In this chapter, we review properties of more complicated multiple-cavity systems that are formed by microspheres assembled in chip-scale structures. The resonant optical properties of such systems can be engineered on the basis of tight-binding WG modes in photonic atoms. In practical systems of coupled cavities, the optical transport properties are strongly influenced by disorder effects, leading to scattering, localization, and percolation of light. The desirable tight-binding properties require selecting more uniform spheres, which can be achieved by novel methods based on using size-selective radiative pressure. Due to controllable dispersions for photons, collective emission and absorption, and enhanced light–matter coupling, such structures can be used for developing coupled arrays of microlasers, ultracompact high-resolution spectrometers, and sensors. The nonresonant properties of such systems are connected through subwavelength focusing of light in chains and arrays of microspheres that can be used in a variety of biomedical applications including ultraprecise laser tissue surgery.

17.1 Introduction

The area of coupled microresonators experienced a significant boost in 1990s when the tight-binding approximation well known in solid-state physics [1, 2] was applied to optical cavities. Analogous to electrons, the tight-binding approximation for photons [3–7] is based on resonant coupling of electromagnetic fields confined to identical "atoms" formed by optical cavities. Several proposals of coupled cavity

V.N. Astratov (✉)
Department of Physics and Optical Science, University of North Carolina at Charlotte, Charlotte, NC 28223-0001, USA
e-mail: astratov@uncc.edu
web:http://maxwell.uncc.edu/astratov/astratov.htm

I. Chremmos et al. (eds.), *Photonic Microresonator Research and Applications*, Springer Series in Optical Sciences 156, DOI 10.1007/978-1-4419-1744-7_17,

devices appeared at that time, including high-order optical filters [8], coupled resonator optical waveguides (CROW) [6], side-coupled integrated spaced sequences of resonators (SCISSOR) [9], and more sophisticated structures [10–16].

Another important factor was connected with the possibility of fabricating coupled cavities with sufficiently high-quality factors ($Q>>10^4$) of individual resonances integrated on the same chip. This included patterned semiconductor microcavities [17], photonic crystal cavities [18–20], and microrings [21–23]. Due to controllable dispersion relations for photons, these structures can be used for developing chip-scale delay lines, spectral filters, and sensor devices.

Although, theoretically, coupled cavity structures can provide almost lossless optical transport [6] in the passbands under the condition $\kappa>>1/Q$, where κ is a coupling constant, this is only true with the assumption that the cavities and their coupling conditions are identical. In real physical structures, the disorder [24–26] becomes to be a dominant factor of optical losses. This remains true even for structures obtained by the best semiconductor technologies [23], such as CMOS, where the standard deviation δ of the individual cavities' frequencies is typically limited to $\sim 0.1\%$ over the millimeter scale distances. An ultracompact optical buffer on a silicon chip [23] is illustrated in Fig. 17.1a. For such structures, losses around 0.3 dB per microring, have been reported [23] for a chain of 100 coupled microrings. There are several techniques that can in principle be used for fine tuning of the individual resonances, such as free carrier injection in p-i-n junctions in semiconductor structures [27] or the use of electro-optical [28] or thermo-optical [21, 29] effects. Application of these techniques to a large number of resonators integrated on a single chip, however, still remains a challenge.

From the time CROW devices were initially proposed [6], it has been well recognized that there is an alternative way of making such structures based on microspheres. Conventional technologies for the fabrication of microdisks, rings, and toroids are essentially planar (2D) technologies, whereas the microspheres can be assembled in arbitrary 3D structures. In addition, the microspheres are characterized with extremely high whispering gallery (WG) mode Q-factors [30–35]

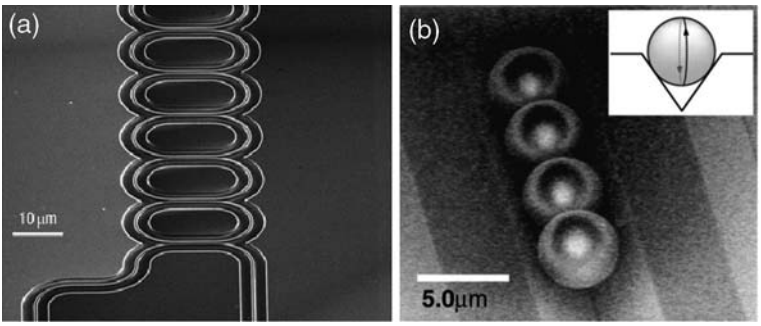

Fig. 17.1 (**a**) Ultracompact optical buffer on a silicon chip [23] obtained by CMOS technology [23]. Reprinted with permission. Copyright 2009 Nature Publishing Group and (**b**) chain of microspheres with coupled WG modes [53] assembled in a groove [53]. Reprinted with permission. Copyright American Physical Society 2009

(>10^4 for 5 μm spheres and up to 10^{10} for submillimeter spheres). The inexpensive microspheres can be manufactured using a variety of materials with different indices of refraction, such as silica [36–38] ($n = 1.45$), borosilicate glass ($n = 1.47$), PMMS [39] ($n = 1.48$), soda lime glass ($n = 1.50$), polystyrene [36–38] ($n = 1.59$), melamine resin ($n = 1.68$), barium titanate glass ($n = 1.9$), titania [39] ($n \sim 2.0$), and even silicon [40] ($n = 3.5$).

These properties of individual microspheres have attracted significant interest in studies of the optical effects in more complicated structures formed by spherical cavities, such as bispheres [41–49], linear chains [50–60], 2D clusters [61, 62], and 3D crystal structures [63, 64]. The strong coupling between WG modes in microspheres has been observed [42–47] along with a number of interesting optical effects. At the same time, it was demonstrated [47, 48, 52] that the standard deviation ($\delta \sim 1$–3%) of the sphere's diameters provided by various manufacturers is too high to achieve efficient WG mode-based coupling.

One way of overcoming this problem is to use the spectroscopic characterization of the WGM peak positions to select size matched microspheres individually [42, 44–46, 53, 54]. This approach has achieved an unprecedented uniformity ($\delta \sim 0.05\%$) of WG mode resonances. Most recently, even higher uniformity ($\delta \sim 0.03\%$) was achieved [65, 66] in bispheres. Future development of this technology is likely to be connected with massively parallel sorting of spheres [67, 68] based on using size-selective optical forces. It has been theoretically demonstrated [68] that when a microsphere is illuminated by an evanescent wave, the optical forces on- and off-WG mode resonance can differ by several orders of magnitude. The force can be extremely size selective ($\sim 1/Q$), and as such, it allows for parallel particle-sorting according to their resonant frequency.

In recent years, the assembly techniques for microspheres have also been dramatically improved. Generally, these techniques belong in three areas: self-assembly, holographic tweezers, and micromanipulation. These include use of self-assembly in pipe-like flows [57–59, 69, 70] for producing long chains of touching cavities, template-directed self-assembly [52, 60, 71, 72] for making arrays and clusters of spheres on grooved substrates, and hydrodynamic flow-assisted self-assembly [64, 73] for synthesizing 3D lattices of spheres. Holographic tweezers [74–79] use a computer-controlled hologram to produce multiple optical traps for microspheres, which can be manipulated to create arbitrary 3D structures. The capability of massively parallel manipulation with hundreds of cavities has already been demonstrated using holographic tweezers, as well as using a method [80] based on optical image-driven dielectrophoresis forces. The last technique requires much smaller optical intensity than the standard optical tweezers. Direct assembly by using a manipulator represents one more possibility for constructing 3D arrays of spheres [81]. It was demonstrated that the gaps between the spheres can be precisely controlled by using stretchable substrates [48].

Particularly interesting results have been obtained in the area of optical transport properties of microsphere resonator circuits (MRCs), where two new concepts were proposed. The first concept concerns the mechanism of transport of WG modes

in 2D and 3D coupled cavity systems with disorder. It was argued [64] that such optical transport can be considered based on an analogy with percolation theory [82, 83] where the sites of the lattice (spheres) are connected with optical "bonds," which are present with probability depending on the spheres' size dispersion. It was predicted that the *percolation threshold* [64] for WG mode-based transport should be achievable in slightly disordered MRCs. Similar optical percolation effects have been recently observed [84, 85] in porous ceramics.

The second concept is connected with the light-focusing properties of microspheres. It has been shown [86–91] that, under plane wave illumination, a single microsphere produces a focused spot, termed "nanoscale photonic jet," with subwavelength dimensions. Small sizes of such photonic nanojets can be used for detecting nanoparticles [87] and for developing high-resolution optical data storage [92]. It has also been suggested [55] that the focusing effects can be periodically reproduced in chains of spheres. Recently, periodical focusing modes, termed "nanojet-induced modes" (NIMs), were directly observed [57–60] in long chains of polystyrene microspheres (>100 cavities).

Thus, MRCs emerged as a novel way of integrating cavities on the same chip, which can provide advantages over conventional structures (microrings, disks, etc.) in specific applications. As an example, size-matched MRCs allow the control of tight-binding photonic dispersions in slow-light devices [53], filters, and array-resonator LEDs. On the other hand, MRCs with size variations can be used for developing novel spectrometers [93] and sensors [94, 95]. The high sensitivity of the WG mode-based sensor devices [96–102] is well known. Multiple-cavity systems can extend the functionality of such sensors. The focusing properties of microsphere chains and arrays can be used for developing biomedical microprobes and laser scalpels with subwavelength spatial resolution.

In this review, we present state-of-the-art technology, theory, and applications in the area of MRCs. In Section 17.2, we consider the tight-binding approximation when applied to microspheres. Section 17.3 is devoted to WG modes in microspheres. Section 17.4 describes the fabrication of MRCs. Section 17.5 explores the optical properties of MRCs. In Section 17.6, we consider applications of MRCs. Finally, in Section 17.7, we draw some conclusions.

17.2 Tight-Binding Approximation for Microspheres

The text book description of tight-binding approximation [1, 2] is based on degeneracy of energy levels in identical uncoupled atoms. For photonic cavities, this translates into the requirement that the dimensionless constant κ, describing the coupling between the identical cavities, should be larger than $1/Q$, where Q is the quality factor of the cavities. As illustrated in Fig. 17.2a, the dispersion relation for photons [6, 7] in infinitely long chains of cavities is given by $\omega_K = \Omega[1 + \kappa \cos(K\Lambda)]$, where K is the wavevector along the chain, Ω is the uncoupled cavity resonance frequency, and Λ is the distance between neighboring cavities. The bandwidth of

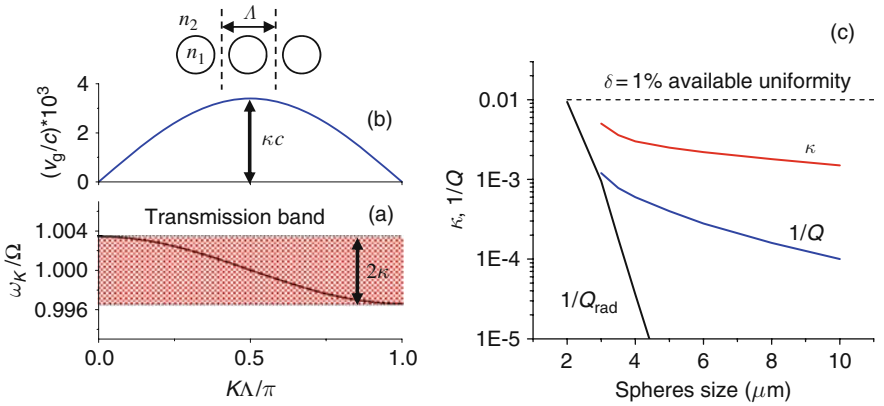

Fig. 17.2 (**a**, **b**) Tight-binding approximation is illustrated for $\kappa = 0.0034$, (**c**) Photonic figure-of-merit demonstrating that the tight-binding approximation is not applicable to commercially available microspheres because of the large variations of the sphere sizes $\delta >> \kappa >> 1/Q$ [103]. Reprinted with permission. Copyright 2009 IEEE

the CROW structure can be calculated as $\Delta\omega = 2\kappa\Omega$. The group velocity can be obtained from this dispersion relation as $v_g = \nabla_K \omega_K = -\kappa\Lambda\Omega \sin(K\Omega)$. As shown in Fig. 17.2b, the group velocity is reduced to κc at the center of the passband, and it approaches zero at the edges of the dispersion diagram. This dispersion is calculated for $\kappa = 0.0034$, which corresponds to the case of touching polystyrene spheres [42, 65] with 4–5 μm diameters.

In the case of chains formed by a finite number (M) of cavities, the tight-binding approximation can be reformulated [24], leading to a discretization of the allowed values of the vector: $K_i = i\pi/(M+1)\Lambda$, where $i = 1,\ldots, M$. Such discrete K_i values have been directly observed in experiments [53] with chains of six size-matched ($\delta = 0.05\%$) polystyrene microspheres.

The photonic figure-of-merit [103] describing a possibility of achieving a coherent tight-binding transport of WG modes in chains of spheres is presented in Fig. 17.2c. In this figure, our experimentally measured [42, 65] values of parameter κ for the polystyrene spheres in air are shown. Coherent coupling phenomena in such systems are achievable under two conditions: (i) $\kappa >> 1/Q$ and (ii) $\kappa >> \delta$. It is seen that the first condition is well satisfied for 2–10 μm spheres. This remains true despite the fact that, in real physical structures, the Q-factors of WG modes in microspheres are significantly reduced in comparison with the estimations (Q_{rad}) based on pure curvature leakage [32, 104, 105], which is shown in Fig. 17.2c. The curvature leakage is a factor limiting Q values only for very small spheres with diameters around 2–3 μm. For larger spheres, the Q values are determined by other factors, such as surface imperfections and material absorption. It should also be noted that if spheres are assembled on the substrate, there are additional factors [104] that affect the broadening of the WG mode resonances, which are discussed in Section 17.3. However, even in this case, as illustrated in Fig. 17.2c, κ exceeds $1/Q$ by approximately an order of magnitude.

Unfortunately, the second condition of coherent transport of WG modes, $\kappa >> \delta$, cannot be satisfied with the commercially available microspheres where $\delta \sim 1\%$, as also illustrated in Fig. 17.2c. In order to achieve tight-binding properties, the spheres should have size variations at least at the level comparable to the dimensionless coupling constant κ. This problem can be solved by using special techniques of selecting size-matched spheres, described in Section 17.5.5.

17.3 Whispering Gallery Modes in Microspheres

Light waves can be trapped in cavities with circular symmetry, such as microrings [21–23], microcylinders [14], and microspheres [41–56], due to total internal reflection of light. Below, WG modes are considered in spherical resonators.

Due to spherical symmetry, WG modes in microspheres are characterized [34, 35] by radial n, angular l, and azimuthal m mode numbers. The radial number, n, indicates the number of WG mode intensity maxima along the radial direction, whereas the angular number, l, represents the number of modal wavelengths that fit into the circumference of the equatorial plane of the sphere. Such waves propagate inside the sphere close to its surface so that they traverse a distance of about $2\pi a$ in a round trip, where a is the sphere radius. The condition of constructive interference of such waves in the cavity with circular symmetry can be approximated as $2\pi a \approx l(\lambda/N)$, where λ/N is the wavelength in the medium with refractive index N. Under the constructive interference condition, standing WG modes are formed [106] in the cavity. This condition can be expressed in terms of the size parameter, $X = 2\pi a/\lambda \approx l/N$.

In an ideal free-standing sphere with a perfect shape, the azimuthal modes represented by m numbers are degenerate. It should be noted, however, that in practice, this degeneracy is lifted by small deformations of the microspheres from the spherical shape. As illustrated in Fig. 17.3, a single sphere on the substrate is rotationally invariant around the z axis playing the part of the polar axis. In this geometry, the fundamental WG modes with $m = l$ are defined [104] in the equatorial plane of spheres parallel to the substrate. Such fundamental modes have the highest Q-factors, due to the fact they are separated from the surface of the substrate by the radius of the sphere. In contrast, the modes with $m << l$ are damped, due to the fact that they have a spatial distribution with the maximum intensity approaching the substrate with the high index of refraction, as illustrated in Fig. 17.3b, c for the WG modes with $n = 2$.

A typical fluorescence (FL) spectrum of a single dye-doped 5 μm polystyrene (N = 1.59) sphere on a glass substrate [65, 66] is presented in Fig. 17.3d. The WG mode peaks with orthogonal polarizations are labeled $TE^n{}_l$ and $TM^n{}_l$, respectively. The peaks in Fig. 17.3d are characterized by $Q = 4 \times 10^3$ for the modes with $n = 1$, which is well below the theoretical limit ($Q > 10^5$) for perfect 5 μm spheres.

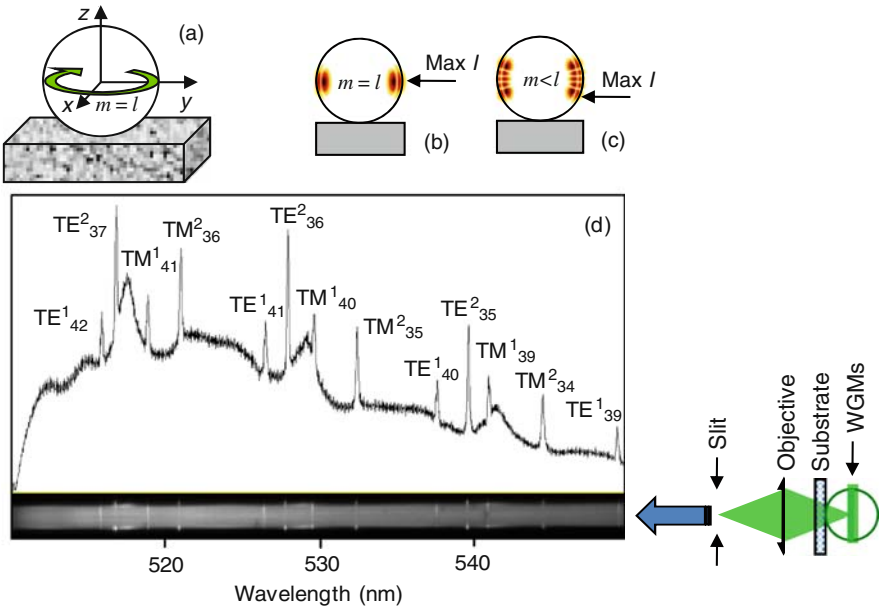

Fig. 17.3 (**a–c**) Schematics of a single sphere on a substrate illustrating intensity maxima distributions for azimuthal modes with different m numbers. (**d**) Fluorescence spectral image and emission spectrum of a single green fluorescent 5.0 μm sphere with $TE^n{}_l$ and $TM^n{}_l$ WGM peaks measured through the transparent substrate [65, 66]. Reprinted with permission. Copyright 2009 Optical Society of America

The positions of fundamental WG mode peaks can be derived from Maxwell's equations solved in spherical coordinates by using the Mie scattering formalism [107, 108]:

$$P\frac{J'_{l+1/2}(NX)}{J_{l+1/2}(NX)} = \frac{N'_{l+1/2}(X)}{N_{l+1/2}(X)}, \tag{17.1}$$

where $P = N$ for TE polarization ($P = N^{-1}$ for TM), and the $(l + 1/2)$ term appears, due to translating the spherical Bessel and Neumann functions to their cylindrical counterparts. By expanding the quantities in (17.1) as an asymptotic series in powers of $(l + 1/2)^{-1/3}$, it is possible to express first terms of the WG mode resonances [108] in terms of the size parameter:

$$NX_{n,l} = l + \frac{1}{2} - \left(\frac{l+1/2}{2}\right)^{1/3}\alpha_n - \frac{P}{\sqrt{N^2-1}} + \ldots, \tag{17.2}$$

where n is the radial number, and α_n are the roots of the Airy function Ai($-z$).

This leads to a quasi-periodic spectrum of WG mode resonances versus l with the frequency separation between the peaks with the same polarization represented by a free spectral range (FSR):

$$\Delta\omega = \frac{c}{2\pi a}\frac{\tan^{-1}\left(\sqrt{N^2-1}\right)}{\sqrt{N^2-1}}. \tag{17.3}$$

The frequency spacing between WG modes having the same n and l but different polarizations can be approximated [109] according to the following formula:

$$\Delta\omega_{n,l}^{\mathrm{TE-TM}} = \frac{c}{2\pi aN}\sqrt{N^2-1/N}. \tag{17.4}$$

For applications in cavity quantum electrodynamics studies, the figure-of-merit for photonic cavities is usually estimated as $\sim Q/\sqrt{V}$, where V is the modal volume. The basic property of WG modes is connected with the relatively small volume occupied by the electromagnetic field of the mode in comparison to the total volume of the cavity [34, 110]:

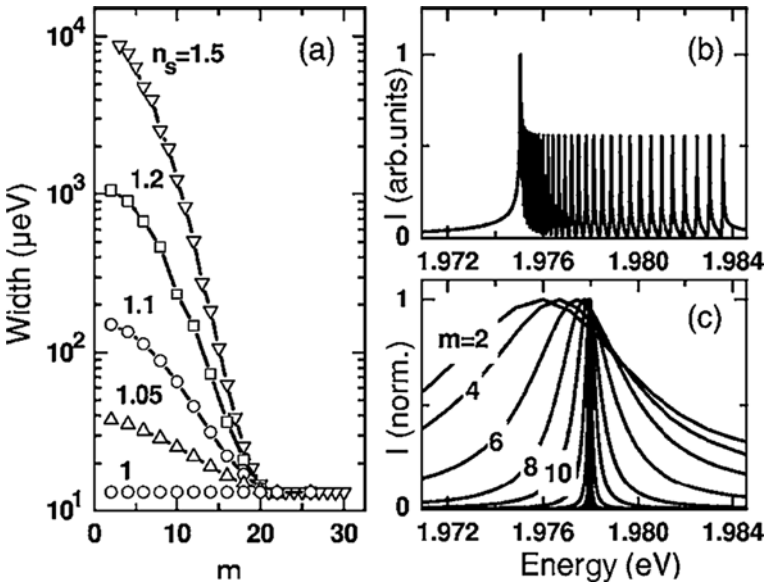

Fig. 17.4 (**a**) Modeling of the $TE^{1}{}_{30}$ WG mode for a polystyrene sphere with $a = 2.25$ μm. Linewidth variation versus the azimuthal mode number m for different index of refraction n_s of the substrate. (**b**) Spectrum resulting from a shape deformation of $|\varepsilon| \sim 0.01$ in absence of the substrate. (**c**) Normalized spectrum of even m modes and $\varepsilon = 0$ in presence of the substrate [104]. Reprinted with permission. Copyright 2009 Optical Society of America

$$V = 3.4\pi^{3/2}\left(\frac{\lambda}{2\pi N}\right)^3 l^{11/6}\sqrt{l-m+1}, \tag{17.5}$$

The degeneracy of azimuthal (m) modes in perfect spheres can be removed by deformations from the spherical shape [111, 112], leading to the appearance of quasi-equidistant closely spaced peaks. An exact solution [104] for deformed ($|\varepsilon| \sim 0.01$) polystyrene microspheres with $a = 2.25$ μm is presented in Fig. 17.4b. The WG mode broadening effect caused by the interaction with the substrate [104] is illustrated in Fig. 17.4a, c. It should be noted that the shape deformation of the sphere breaking the symmetry around the z-axis can mix the modes of different m, thus giving rise to a broadening of all modes, due to tunneling to the substrate. These effects are likely to be responsible for the WG linewidth broadening observed in the experimental spectra of microspheres.

17.4 Fabrication of Microsphere Resonator Circuits

In contrast to "hard" semiconductor in-plane fabrication techniques, the synthesis of MRCs relies on a variety of soft condensed matter methods. Soft matter structures and devices are often inexpensive which allows one to quickly iterate and modify designs [113, 114]. These methods can be divided into three major categories considered above: self-assembly, optical tweezers, and micromanipulation.

17.4.1 Self-Assembly

During the last two decades, the techniques of self-assembly of spheres with submicron dimensions ~0.2–0.5 μm have been developed for obtaining 3D photonic crystal structures. These techniques include slow sedimentation in gravity for growing synthetic opals [115–118], vertical deposition techniques [119, 120] for obtaining well-ordered layers of spheres, template-directed colloidal deposition techniques [71, 72, 121–123] for synthesizing well-ordered arrays of spheres on patterned substrates, techniques of 3D self-assembly in hydrodynamic flow [73], and the techniques of self-assembly in pipe-like flows [69, 70] for producing long chains of touching cavities.

The size of the spheres used in MRCs (~2–10 μm) is larger than in opal-like structures by an order of magnitude. For such enlarged spheres, the sedimentation times are orders of magnitude shorter than those for conventional opals. This does not allow obtaining ordered structures by conventional sedimentation techniques on flat substrates. The quality of ordering can be improved by using dents, grooves, or other patterns [52, 71, 72] fabricated in the substrate. The spheres tend to occupy lowest energy positions in the patterned templates which results in better ordered structures. The ordering of spheres can be further improved [60] by using effects of

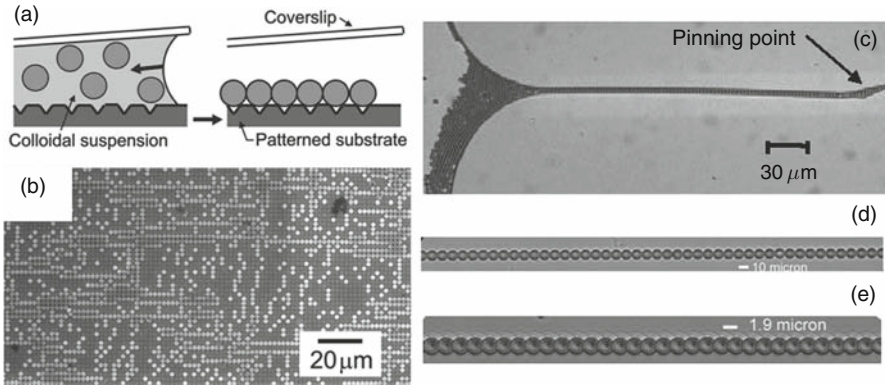

Fig. 17.5 (**a**, **b**) Schematic of the self-assembly by slowly moving front of liquid and SEM image of the microspheres on a patterned substrate [60]. Reprinted with permission. Copyright 2009 Optical Society of America. (**c**–**e**) Self-assembly in pipe-like flows on a flat substrate [57–58]. Reprinted with permission. Copyright 2009 American Institute of Physics

packing of microspheres by a slowly moving front of evaporating liquid illustrated in Fig. 17.5a, b.

Another technique of self-assembly [57–59] suitable for fabrication of straight chains of spheres in a touching position on a flat substrate is illustrated in Fig. 17.5c–e. In this method, the liquid film with spheres is sandwiched between two hydrophilic glasses. The evaporating liquid film forms pipelike flows, stretching from massive deposits of microspheres to "pinning" points nucleated by bigger spheres or by the defects on the substrate. Evaporation of microflows in a lateral direction leads to the formation of straight and long chains of touching spheres. As shown in Fig. 17.5d, e, this technique allows obtaining perfectly aligned chains [57, 58] with less than 1 defect per 100 spheres. Similar results can be obtained by a modified technique [124] where the self-assembly of microspheres occurs in the proximity of a glass rod placed on a flat substrate. In this technique, during the evaporation of the solvent, the spheres are dragged into the meniscus of the suspension between the glass rod and substrate. Ordered chains of microspheres have been obtained after complete solvent evaporation, [124].

Fabrication of 3D lattices of spheres can be achieved by using hydrodynamic flows of microspheres in confined geometries [64, 73]. In this technique, the suspension of microspheres is injected into a cell with the porous walls allowing the liquid portion of the suspension to drain through, while retaining the spheres inside the cell. The realization of this method is straightforward for enlarged spheres [64] used in MRCs, since the size of the pores in the walls should be smaller than the size of the spheres. The thickness of the 3D lattice of spheres is determined by the thickness of the cell. An ultrasonic bath is used to speed up the synthesis of 3D structures. This process usually yields polycrystalline samples containing sizable ($\sim$100 μm) domains with face-centered-cubic (FCC) packing of the microspheres.

17.4.2 Optical Tweezers

An optical trap can be created [125] by focusing a laser beam to a diffraction-limited spot using a high numerical aperture objective lens. As schematically illustrated in Fig. 17.6a, the strong light gradient near the focus creates a potential well, in which a particle with a refractive index higher than that of the surrounding aqueous medium is trapped [126]. By using multiple optical traps, up to 400 particles can be simultaneously manipulated [126, 127]. An example of manipulation with multiple polystyrene microspheres [127] is shown in Fig. 17.6b. The arrays of microspheres can be held in position using holographic tweezers [74, 75]. After that, the surrounding medium can be gelled to fix the spheres in place [76]. Alternatively, the spheres can be forced together using holographic tweezers and caused to adhere by controlling the colloidal interaction in the system [79]. An advantage of using multiple traps is connected with a possibility of direct assembly of 3D structures with arbitrary configurations of microresonators [78, 79]. An example of a FCC crystal structure [79] formed by 3 μm polystyrene microspheres is illustrated in Fig. 17.6c.

An interesting method [80] has been developed recently in which particle manipulation is achieved, due to the combined effect of an electric field and illumination. This optical image driven dielectrophoresis technique permits

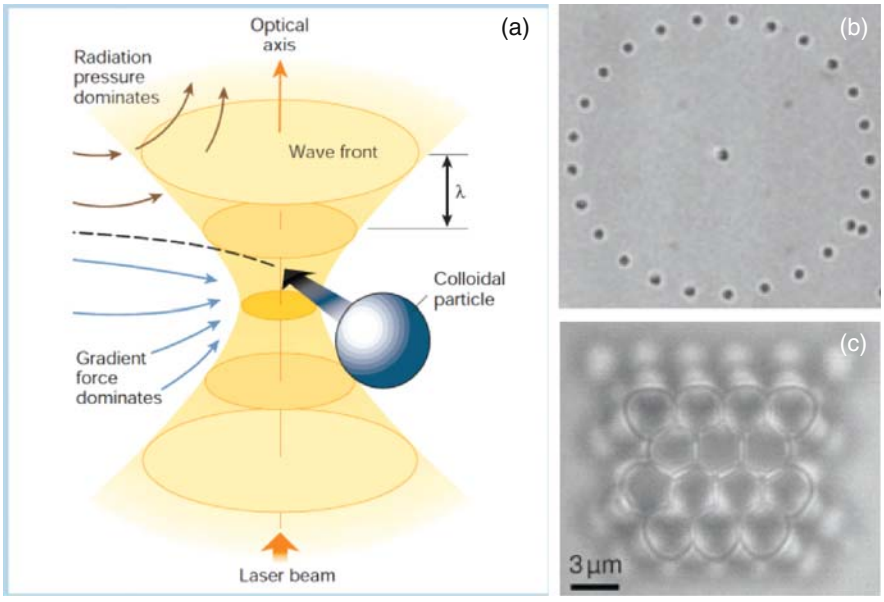

Fig. 17.6 (**a**) Schematic of the focused beam with a colloidal particle drawn toward the focus [126]. Reprinted with permission. Copyright 2009 Nature Publishing Group. (**b**) Water-borne 0.8 μm polystyrene spheres trapped in a plane and reconfigured with dynamic trapping patterns [127]. Reprinted with permission. Copyright 2009 Elsevier. (**c**) Three layers of FCC structure made from 3 μm silica spheres [79]. Reprinted with permission. Copyright 2009 Optical Society of America

high-resolution patterning of electric fields on a photoconductive surface for manipulating single particles. It requires 10^5 times less optical intensity than optical tweezers.

17.4.3 Micromanipulation

Small-scale structures containing a limited number of microresonators can be fabricated by micromanipulation. The mechanical microassembly requires the position of the spheres on the substrate to be stable. This can be achieved by using patterned substrates, as shown in Fig. 17.7a. The nanorobotic manipulation of 0.9 μm spheres using SEM can obtain perfectly ordered structures as seen in Fig. 17.7a. The disadvantage of nanorobotic manipulation is connected with the fact that it is a time-consuming process.

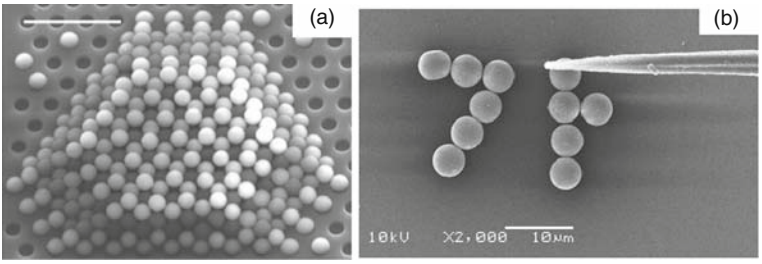

Fig. 17.7 (**a**) Nanorobotic manipulation in SEM showing six layers of body-centered-cubic structure formed by 0.9 μm spheres assembled on a patterned substrate [81]. Reprinted with permission. Copyright 2009 Wiley-VCH. (**b**) First Korean letter formed by 5 μm polystyrene microspheres manipulated by a tapered fiber [65]. Reprinted with permission. Copyright 2009 Optical Society of America

It should be noted that micromanipulation is greatly simplified when using large spheres as in MRCs. The micromanipulation can be provided by tapered fibers or metallic micro-needles connected with hydraulic micromanipulators. An example of a structure formed by 5 μm polystyrene microspheres on a flat glass substrate [65] is represented in Fig. 17.7b. The spheres are attached to the substrate, due to a surfactant with gluing properties used by the manufacturer of microspheres. These techniques are convenient for building bispheres or small clusters of spheres. They can also be used for sorting size-matched spheres as described in Section 17.5.

The variation of the inter-sphere gaps can be achieved by using the substrates with elastomeric properties [48]. This technique was developed for PDMS substrates obtained with a reduced concentration of a cross-linker to provide increased elasticity. Using this technique the inter-resonator gaps were controlled [48] in the 0–2.5 μm range with 20 nm accuracy.

17.5 Optical Properties of Microsphere Resonator Circuits

In recent years, the focus of theoretical studies of coupled cavities has been on their spectral properties. Coupling between identical cavities is well studied at present time, especially for 2D systems, such as coupled microrings and microdisks [8–16]. The degeneracy of WG modes can be lifted in such systems that result in the spectral properties depending on the configuration of cavities and on the strength of their coupling. It is shown that various types of coupled microresonators demonstrate common spectral properties. Examples of such coupled systems include biatomic photonic molecules formed by planar semiconductor microcavities [128], patterned microcavities [17], photonic crystal cavities [129], microrings [11], microdisks [130], and microspheres [41–49]. Integration of several identical cavities in symmetric photonic molecules leads to the formation of high-Q supermodes [131]. It has been shown that the photonic dispersions can be modified in infinite 2D arrays of coupled microrings [132]. In structures with positional disorder of cavities, the collective resonances of multiple cavities can be calculated using multipole formulation [133]. Some of these results are reviewed in more detail in Chapter 16 of this book.

In this section, we focus on the optical properties of coupled microspheres, including both spectral and transport effects. We consider effects which are essential for developing MRCs, such as the role of the substrate, optical losses in size-disordered structures, efficiency of coupling between size-mismatched cavities, percolation of WG modes in 2D and 3D structures, effects of periodical focusing of light in chains of spheres, and methods of selecting spheres with particularly high size uniformity.

17.5.1 Role of Substrate: Fundamental WG Modes

Similar to individual spheres considered in Section 17.3, in coupled cavity structures, the interaction with the substrate plays an important role in the optical transport properties. Contact with a high-index substrate leads to a damping of many WG modes in individual spheres. This factor complicates the theoretical understanding of the WG tight-binding effects in such structures. Indeed, in the absence of the substrate, a bispherical system (as the simplest example) is characterized [43, 49] with a polar axis connecting the centers of two cavities, which means that the single cavity fundamental WG modes are defined in the planes perpendicular to such polar axis, as shown in Fig. 17.8a. If a bisphere is assembled on a substrate, however, such fundamental modes should be damped, due to their leakage in the substrate. It is well known [65, 66, 104] that only WG modes with the intensity maxima separated from the substrate have sufficiently high Q-factors. In the case of flat substrates, this favors WG modes located in the equatorial plane of spheres parallel to the substrate, shown in Fig. 17.8b. In the case of spheres assembled in V-grooves, this factor favors WG modes in a plane perpendicular to the substrate [53], as illustrated in the inset of Fig. 17.1b.

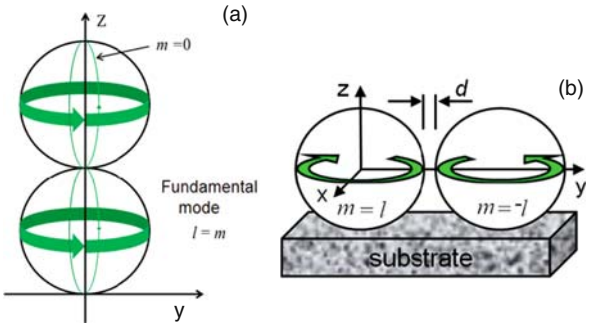

Fig. 17.8 (**a**) Fundamental modes for free-standing bispheres and (**b**) bisphere on a substrate [134]

In this review, the uncoupled WG eigenstates of the coupled cavity system are introduced in a similar manner as in the case of a single sphere on the substrate, as illustrated in Fig. 17.8b. This approach describes a weak coupling between the cavities when the perturbation of WG modes caused by their interaction is small. It should be noted that, in a strong coupling regime, the hybridization effects for WG modes in the presence of the substrate are not well studied at present.

17.5.2 Optical Transport in Disordered Structures

As shown in Section 17.2 in overcoupled structures ($\kappa >> 1/Q$) formed by relatively uniform ($\kappa >> \delta$) resonators, the optical transport should be very efficient. The last condition, however, is not satisfied in real physical assemblies of microspheres. This problem is generic for all types of chip-scale coupled cavity structures including microrings obtained by the precise CMOS technology [23].

The cavities' size variations reduce the efficiency of evanescent coupling between their WG modes. As a result, WG modes are partially reflected at the contact points between the spheres, leading to the localization of light [24–26] and scattering losses. The average losses (~0.3 dB per ring) have been reported [23] for silicon microrings with ~0.1% standard size variations.

In MRCs, the transport of WG modes is expected to be less efficient due to larger standard deviation of the spheres' diameters ~1%. The measurements of losses were performed [52, 58] in long chains of 5 μm polystyrene microspheres, as illustrated in Fig. 17.9. In these experiments, a dye-doped sphere was used as a source (S) of evanescently coupled WG modes, as shown in Fig. 17.9a. The transport of light at different wavelengths was studied using spectral scattering images, shown in Fig. 17.9b. As illustrated in Fig. 17.9c, in the first few spheres adjacent to the source, the average propagation loss at the WG mode wavelengths is found to be ~3 dB per sphere. The optical transport was found to be more efficient at the wavelengths away from the resonance with WG modes. This nonresonant mechanism of optical transport is considered in Section 17.5.6.

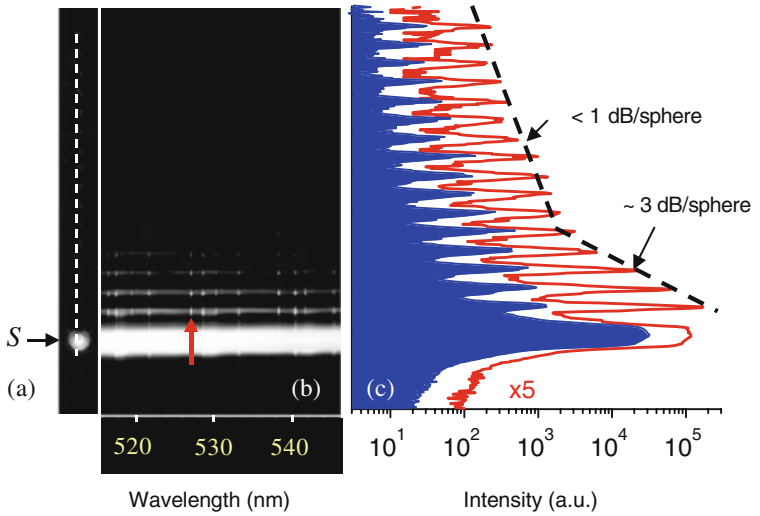

Fig. 17.9 Scattering spectroscopy [58]: (**a**) image of the chain in contact with the dye-doped S sphere with the central section indicated by the *dashed line*, (**b**) scattering spectral image at the central section in the spheres equatorial plane, and (**c**) intensity distribution measured at 527.3 nm $TE^{1}{}_{41}$WG mode peak (*solid line*) and away from the WG peaks at 525.0 nm (distribution with the *filled area* under the curve). The *dashed lines* are to guide the eye [58]. Reprinted with permission. Copyright 2009 American Institute of Physics

17.5.3 Efficiency of Coupling Between the Size-Mismatched Cavities

The simplest system for studying the efficiency of evanescent coupling between microcavities is represented by biatomic photonic molecules. It is well known that the classical system of strongly coupled cavities can be considered by analogy to a quantum mechanical strongly driven two-level system [135]. One of the examples of such systems is represented by microcavity polaritons [136], where excitons confined in quantum wells are strongly mixed with the optical cavity modes. Each polariton mode, $|p\rangle$, is a linear combination of an exciton, $|e\rangle$, and a cavity photon, $|l\rangle$: $|p\rangle = c_e|e\rangle + c_l\,|l\rangle$. Exactly at resonance, both polaritons consist of equal mixtures of the exciton and photon states, so $c_e = \pm c_l = 2^{-1/2}$. The symmetric and antisymmetric modes are then split by a finite energy, known as the vacuum Rabi splitting [137]. When the system is detuned from resonance, the mixture is not equal, with one mode predominantly excitonic in character ($c_e \to 1$, $c_l \to 0$) and the other predominantly photonic ($c_e \to 0$, $c_l \to 1$) [138, 139]. A similar approach can be used for photonic molecules, where the fractions of individual cavity modes in the strongly mixed molecular states define the coupling efficiency between photonic atoms.

It should be noted that the behavior of coupled cavities in the vicinity of energy level anticrossing exhibits several interesting effects, including the formation of so-called exceptional points [140], where the complex eigenvalues of the

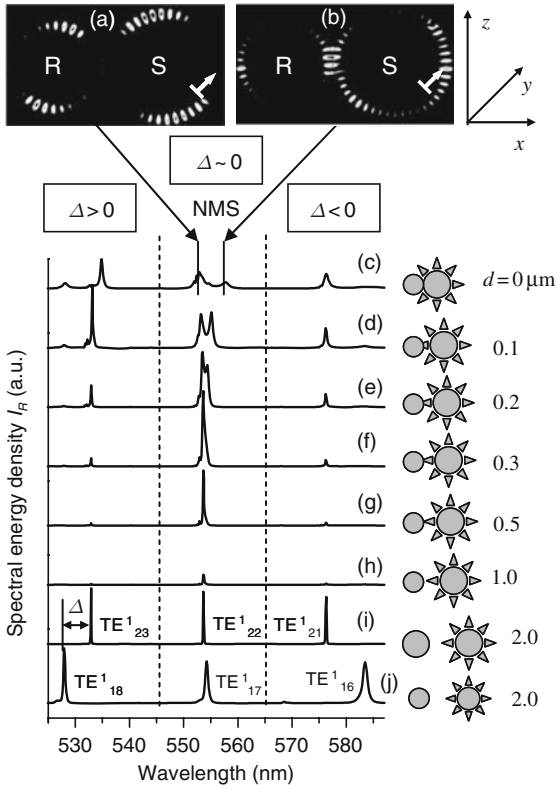

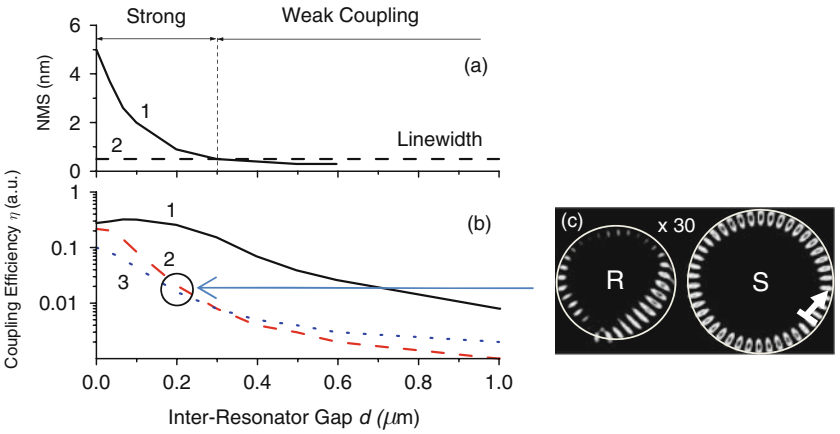

Fig. 17.10 (**a**) Antibonding and (**b**) bonding states. (**c**–**h**) Spectral energy density in receiving (*R*) sphere for different gaps (*d*). (**i**, **j**) spectra of WG eigenstates [47]. Reprinted with permission. Copyright 2009 American Institute of Physics

Fig. 17.11 (**a**) Normal mode splitting (NMR) in resonant case as a function of *d* (*line 1*). (**b**) The coupling efficiency (η) as a function of *d* for different detuning (Δ) [47]: 1–Δ = 0.5 nm, 2–Δ = 5 nm, 3–Δ = –7.5 nm. (**c**) Distorted mode in the *R* sphere in detuned cases [47]. Reprinted with permission. Copyright 2009 American Institute of Physics

corresponding levels coalesce. It also includes the formation of long-lived, scar-like modes [141]. For coupled microdisks, the behavior in the vicinity of resonance crossing has been studied using numerical modeling [142, 143] and also experimentally [144, 145].

For size-mismatched (3.0–2.4 μm) spheres with index 1.59, the coupling effects were studied [47] using 3D FDTD modeling, as illustrated in Fig. 17.10. One of the spheres was used as a source (*S*) of WG modes. The spectra of electromagnetic energy (I_R) were calculated in a second receiving (*R*) sphere. The effect of the substrate was mimicked by launching the WG modes in the plane containing the axis of the bisphere. Due to the fact that each resonator produces its own comb of uncoupled WG mode peaks in Fig. 17.10i, j, it was possible to study coupling phenomena for various detuning (Δ) between closest resonances. The regime of strong coupling is evident in all cases under the spheres' touching condition ($d = 0$), as illustrated by classical bonding and antibonding molecular states in Fig. 17.10a, b. Increasing the separation between the cavities leads to a gradual transition to weak coupling shown in Fig. 17.11a.

As a measure of the total energy (E_R) deposited in the *R* cavity, the area under the spectral peaks was used. A rough estimate of the coupling efficiency (η) was obtained by normalizing E_R by similarly estimated energy (E_S) in the *S* sphere: $\eta = E_R/E_S$. The results of calculating η for different detuning, Δ, as a function of *d* are summarized in Fig. 17.11b. It is seen that, in a contact position, the coupling efficiencies are typically ~0.1–0.2, regardless of detuning.

In strongly detuned cases, the modes induced in the *R* sphere exhibit an irregular noncircular shape, as illustrated in Fig. 17.11c. Such weakly coupled modes have a shape that can be continuously adjusted to variations in frequency of the WG mode in the *S* sphere [47]. Such coupling between a discrete energy state (true WG mode in the *S* cavity) and a continuum of irregular modes in the *R* cavity resembles Fano resonance [146] phenomena observed in photonic crystal waveguides [147] and side-coupled waveguide-cavity [148] systems.

17.5.4 Percolation of WG Modes in 2D and 3D Structures

The optical transport in 2D and 3D structures [61–64] is a much more complicated phenomenon compared to that in single chains of cavities [50–60]. In close-packed 2D arrays of spheres, each cavity has six neighbors. In close-packed 3D lattices, each cavity has 12 neighbors. This means that the probability of finding a neighbor with highly efficient WG mode coupling is higher in the 2D case, and much higher in the 3D case, compared to bispheres (one neighbor) or chains (two neighbors). The optical transport in such 2D and 3D systems can be considered as analogous to the *bond percolation theory* [82, 83]. This is illustrated in Fig. 17.12a for a square lattice of sites connected with bonds with probability *p* [83]. If *p* is smaller than a critical value, p_c, termed the bond *percolation threshold* ($p_c = 0.5$ for the lattice of square sites), only finite clusters of connected sited can be formed. However, if *p* exceeds this critical value, an infinite or giant cluster is formed, which means that it

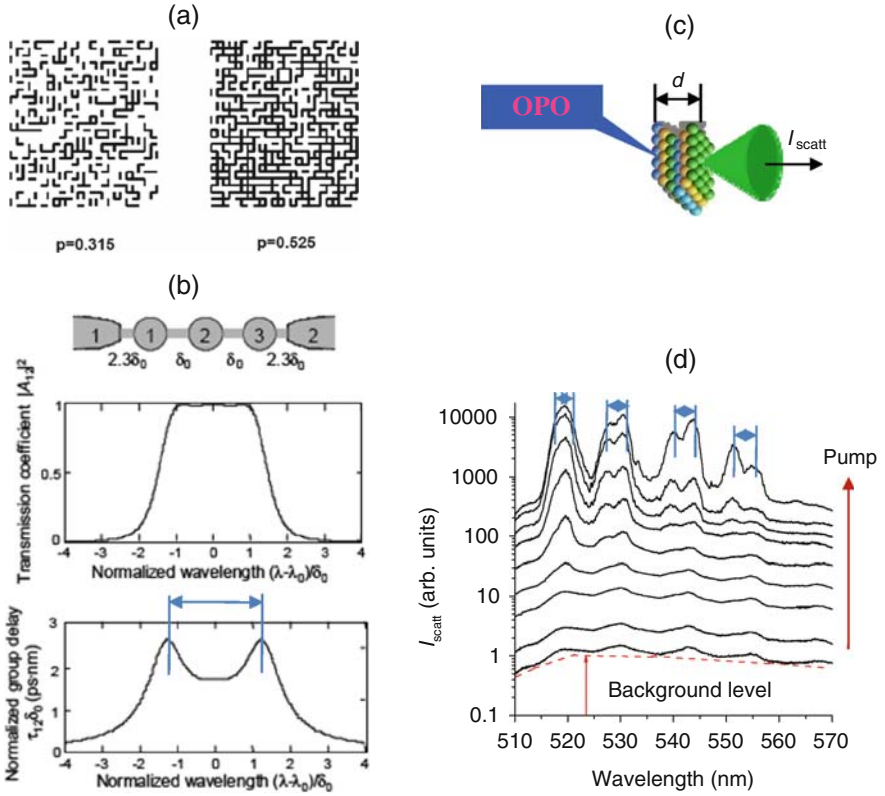

Fig. 17.12 (**a**) Illustration of bond percolation in 2D [83]. Reprinted with permission. Copyright 2009 American Physical Society. For $p = 0.315$ (*left*), which is below the percolation threshold, $p_c = 0.5$, the connected nodes form isolated clusters. For $p = 0.525$ (*right*), the largest cluster percolates. (**b**) Optical passband and two peaks of the normalized group delay in a chain of uniform microresonators [10]. Reprinted with permission. Copyright 2009 Optical Society of America. (**c**) Optical set up for FL transmission measurements in 3D lattices of dye-doped microspheres. (**d**) FL transmission spectra demonstrating double peak structures at high pumping conditions [64]. Reprinted with permission. Copyright 2009 Optical Society of America

should be possible to propagate the entire thickness of the lattice through the system of connected bonds.

In the case of optical cavities, the probabilities of the bonds are represented by the WG mode coupling efficiencies. As it was already stated, the transport between identical cavities can be very efficient, leading to the formation of a passband in transmission [6, 7, 10] shown in Fig. 17.12b. It also leads to the formation of two peaks of normalized group delay [10, 12] at the edges of the passband. Such *double peak structures* appear due to increased dwelling time of light in the structure, which is caused by the partial reflections of light between the cavities.

These phenomena were studied [64] in 3D lattices formed by closely packed dye-doped polystyrene microspheres. By using optical pumping, the WG modes

were locally excited in multiple spheres located in the near-surface region of the sample, as illustrated in Fig. 17.12c. At small pumping levels these WG modes can be detected from the opposite face of the sample as inhomogeneously broadened peaks superimposed on a broad background, as shown in Fig. 17.12d. At high pumping levels, each peak was found to split into a double peak structure, very similar to that is shown in Fig. 17.12b. The magnitude of splitting was found to be similar to that in the calculated [43, 47] and experimental [42, 44–46, 65, 66] spectra of resonant bispheres with comparable size. These results can be explained [64] by the presence of finite clusters of size-matched spheres inside otherwise disordered samples, which are well connected at WG mode wavelengths. These results also suggest the possibility of achieving an "optical percolation threshold" for WG mode-based transport in such systems by selecting spheres with smaller standard size variation δ. It is interesting that a similar approaches to understanding optical transport properties have been applied to pores ceramics [84, 85], where the optical percolation threshold has been experimentally observed.

17.5.5 Selection of Size-Matched Spheres

The straightforward way of selecting size-matched spheres is based on their micromanipulation, controlled by spectroscopy [42, 44–46, 53, 54]. Sorting of microspheres with $\delta \sim 1/Q$ can be obtained by this technique. For diatomic molecules formed by almost indistinguishable classical "atoms," a series of optical coupling effects has been observed. First, this includes observation of normal mode splitting for fundamental WG modes [42, 44–46] with the orientation determined by the interaction with the substrate, as it is discussed in Section 17.5.1. Second, the lifting of the degeneracy of azimuthal WG modes can be directly observed in such structures. For photonic molecules (PMs) with $\delta \sim 0.07\%$ assembled in microwells, it was observed in experiments with off-axis excitation and detection [46], as illustrated in Fig. 17.13a, b. For PMs with $\delta \sim 0.03\%$ assembled on the substrate [65, 66], the lifting of degeneracy of azimuthal modes results in peculiar shapes resembling kites in the spectral images, as illustrated in Fig. 17.13c. Such kites give direct spectral evidence for maximal coupling of WG modes in the equatorial plane of spheres determined by the substrate. The coupling constant κ was quantified [65, 66] for such modes with respect to sphere sizes and modal numbers.

Future development of MRC technology is likely to be connected with massively parallel sorting of spheres [67, 68] based on using size-selective radiative pressure. It has been theoretically predicted [67] that when a microsphere is illuminated by an evanescent wave, the optical forces on- and off-WG mode resonance can differ by several orders of magnitude, as illustrated in Fig. 17.14. This technique allows for potentially accurate size-selective manipulation, as well as parallel particle-sorting according to their size or resonant frequency with $\delta \sim 1/Q$ size

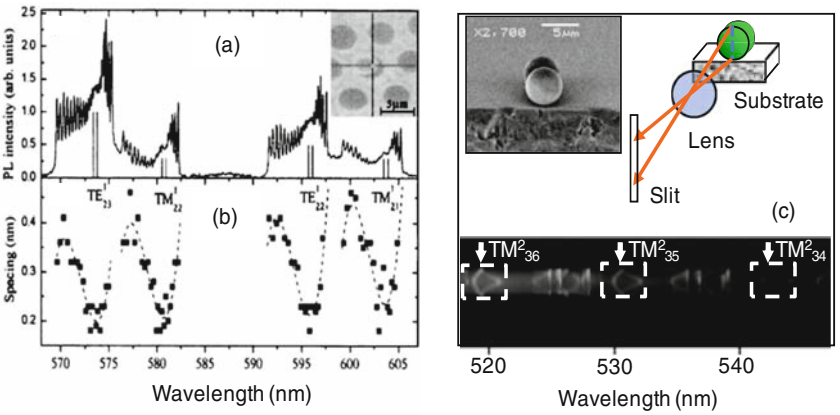

Fig. 17.13 (**a**) The photoluminescence (PL) spectra of the diatomic PM ($\delta \sim 0.07\%$) in a microwell measured with off-axis excitation and detection [46]. Reprinted with permission. Copyright 2009 American Physical Society. *Inset*: microscope image of the PM. The *dark cross* indicates the excitation position. (**b**) The spacing between neighboring peaks. (**c**) Diatomic PM ($\delta \sim 0.03\%$) assembled near the edge of the substrate, experimental configuration and spectral image illustrating shapes resembling kites near each WG mode resonance. For clarity this is illustrated by *dashed boxes* for the second-order TM peaks [65, 66]. Reprinted with permission. Copyright 2009 American Physical Society

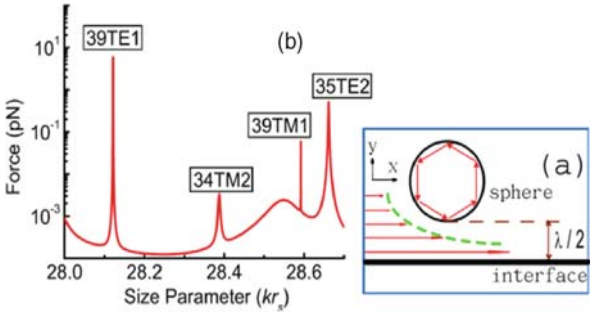

Fig. 17.14 The optical force acting on a microsphere with $a \sim 2.317$–2.375 μm at $\lambda = 520$ nm. (**a**) A schematic illustration of how the evanescent wave excites a WG mode. (**b**) For the sphere's dielectric permittivity $\varepsilon_{\text{sphere}} = 2.5281 + 10^{-5}i$. The incident wave is an *s*-polarized evanescent wave with $k_{||}/k = 1.25$ and $I_0 = 10^4$ W/cm^2, where $k_{||}$ is the component of the wavevector parallel to the wave's propagating direction [67]. Reprinted with permission. Copyright 2009 American Institute of Physics

uniformity. One of the challenges in developing this technique is due to the reduction of *Q*-factors for WG modes in spheres immersed in a liquid. Developing these techniques will have a profound impact on modern photonic integration technologies, due to controllable tight-binding photonic dispersions in such structures and a wide variety of structures and devices which can be assembled using size-matched microspheres.

17.5.6 Nonresonant Light-Focusing Properties of Chains of Spheres

While previous sections considered spherical cavity resonant properties, these cavities can also be used to focus light having a broad range of wavelengths. For sufficiently large ($a>>\lambda$) microspheres, the focusing effects follow the laws of geometrical optics [149]. For spheres with radii comparable to the incident radiation wavelength, near-field optical effects become an important which result in extremely small sizes of the focused spots [150–154]. It has been demonstrated that when the focus point is close to the surface of the sphere, the beam width in the focus area becomes smaller than the wavelength over a distance of a few wavelengths [86–91]. This unique distribution of electromagnetic intensity has been termed a photonic nanojet [86] based on its appearance.

It has been shown that the nature of electromagnetic field outside the sphere is strongly dependent on its index of refraction [55]. For index $N = 1.59$, the focused beam possesses not only evanescent fields, but also radiative-mode components, as illustrated in Fig. 17.15a for a plane wave-illuminated ($\lambda = 400$ nm) sphere with $a = 1.5$ μm. In contrast, for $N = 1.8$, the optical power within such a microsphere is totally internally reflected, and it can tunnel out of the sphere through evanescent coupling, as illustrated in Fig. 17.15b.

It has been suggested that, in chains of coupled cavities, this should lead to two different mechanisms [55] of optical transport: nonresonant micro-lensing,

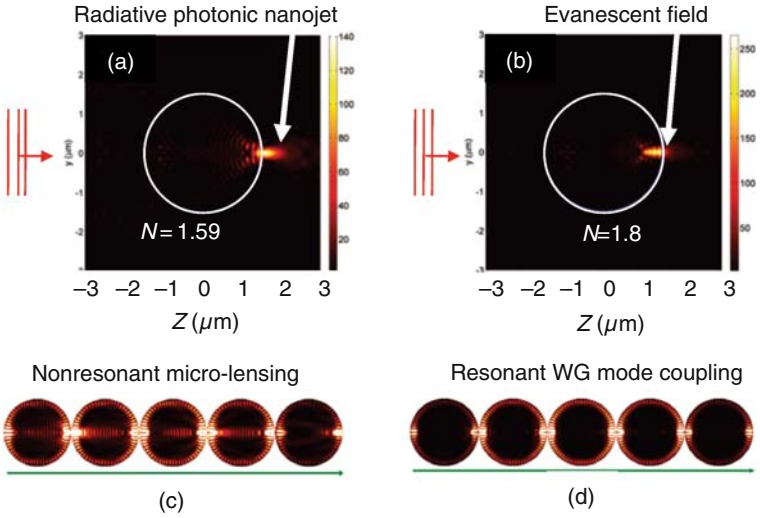

Fig. 17.15 Visualization of a photonic nanojet [55] emerging at the shadow-side surface (*circle*) of a dielectric microsphere ($a = 1.5$ μm) with the refractive index N of (**a**) 1.59 and (**b**) 1.8. The sphere is illuminated by a plane wave with $\lambda = 400$ nm. Electric field intensity distributions of a chain of five touching microspheres that have a refractive index of (**c**) 1.59 at $\lambda = 429.069$ nm and (**d**) 1.8 at $\lambda = 430.889$ nm [55]. Reprinted with permission. Copyright 2009 Optical Society of America

illustrated in Fig. 17.15c, and resonant WG mode-based coupling, shown in Fig. 17.15d.

Such periodical focusing effects have been directly observed [57–60] in the long chains of touching polystyrene microspheres with 2–10 μm sizes. As illustrated in Fig. 17.16a, b, the quasi-periodical series of nanojets was visualized [57] by using imaging spectroscopy and microscopy.

One of the interesting results, which can lead to applications of coupled microspheres, is the progressively smaller focused spots' sizes observed along such chains, as illustrated in Fig. 17.16b,c. It was shown that the diffraction-limited spot sizes can be obtained in such structures for chains containing less than ten spheres [57]. The period of these quasi-periodic nanojet-induced modes (NIMs) propagating in such structures was found to be equal to the size of two spheres with index 1.59 [58], as illustrated in Fig. 17.16d. These modes are most efficiently coupled to the collimated incident beams. For noncollimated incident beams, the maximum losses ~2–3 dB per sphere occur in the first few spheres, as shown in Fig. 17.16e. Further along the chain, the losses become progressively smaller, reaching a very small level ~0.08 dB per sphere [58]. For this reason, NIMs are the most favored modes surviving in the long straight chains of coupled microresonators with disorder. Such focusing effects take place in a broad range of wavelengths, which can be used in a variety of biomedical applications requiring a combination of tight focusing and high optical output.

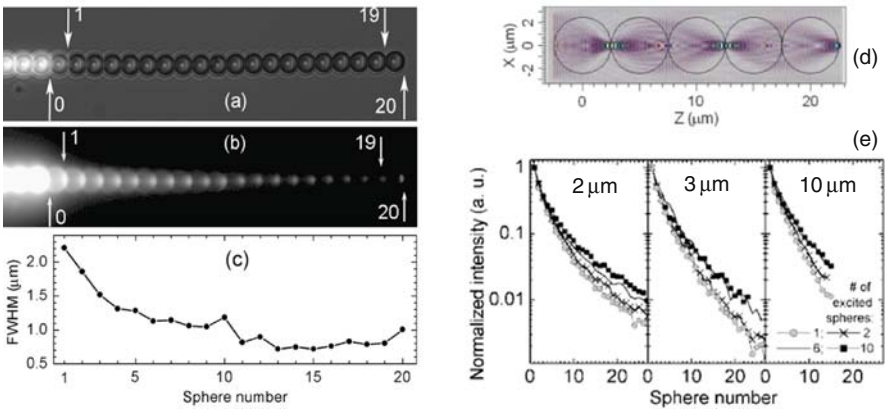

Fig. 17.16 (**a**) Coupling of light in the chain using FL spheres as a local source [57]. Reprinted with permission. Copyright 2009 Optical Society of America. (**b**) Scattering image illustrating periodical focusing by the spheres with $a = 1.45$ μm with progressively smaller spot sizes. (**c**) Cross-sectional width of the spots illustrating their diffraction-limited dimensions. (**d**) Periodical focusing in 5 μm spheres with $N = 1.59$ obtained by FDTD numerical modeling. (**e**) Attenuation of the nanojets intensities along the chains formed by 2, 3, and 10 μm spheres [58]. Reprinted with permission. Copyright 2009 American Institute of Physics

17.6 Applications of Microsphere Resonator Circuits

The existing methods of fabrication of coupled cavities have a number of drawbacks, which limit the functionality of the resulting structures. For example, while lithography is a flexible technique for generating different optical structures, the technique is essentially two-dimensional, meaning that many steps must be repeated to create 3D structure. Microspheres, on the other hand, can be assembled in arbitrary 3D structures using a variety of inexpensive methods such as self-assembly, optical tweezers, or micromanipulation.

Most importantly, the microspheres can be pre-sorted with the size uniformity [42, 44–46, 65–68], $\delta \sim 1/Q$, which is not available for conventional techniques of fabrication of microrings, disks, toroids, or photonic crystal defects [21–23, 27–29, 155]. This extraordinarily high level of size uniformity allows developing novel structures and devices with unique functionality.

A particularly interesting area is represented by the resonant optical forces in systems of size-matched spheres. The use of optical forces in optomechanical cavities [156] and integrated photonic circuits [157, 158] has attracted significant attention recently due to their novel physical properties and applications in nanomechanical resonators. It is known that even size-disordered microspheres can be assembled in relatively regular arrays [159] using evanescent optical fields. In size-matched microspheres, the resonant optical forces between coupled WG resonators are expected to be much stronger [160], which should result in the development of new methods of assembling optically bounded structures and devices.

Resonant positions of WG modes in size-sorted cavities open new possibilities for developing laser applications with advanced functionality. Examples include bistable [161] and single-mode [162] lasing, observed in different coupled cavity structures. Another example is represented by coherently driven high-power laser arrays, such as VCSELs [163–165]. A monolayer of close-packed microspheres behaves as an array of laterally coupled microlasers [64]. Such arrays of active (dye- or Er-doped) size-matched microspheres can be integrated with the semiconductor lasers, planar waveguides, or fibers, in order to develop coherently driven sources of light with applications in communications, imaging, and other fields of optical engineering.

Tight-binding photonic dispersions can be used for developing high-order spectral filters [8] and tunable delay lines [6]. It should be noted that, in recent years, there has been significant progress in developing designs [166, 167] and applications [21–23, 168, 155] of coupled microrings. As an example, the thermal tuning of silicon oxinitride (SiON) microrings permitted the realization of an error-free, continuously tunable delay at 10 Gbit/s in a reconfigurable on-chip delay-line [168]. The practical realization of such structures is, however, complicated by the necessity to provide a final tuning of the individual cavities. Size-sorted microspheres can provide advantages in such applications. The control of the tight-binding photonic dispersions has been demonstrated [53] in linear chains of size-matched ($\delta \sim 0.05\%$) spheres.

Another interesting area of applications of MRCs is connected with the control of light–matter interaction in coupled cavities [169] through constructive interference of the resonator decays. It has been shown [169] that the temporal decay rate of a parallel resonator chain is proportional to the number of resonators, while the intensity of the decay is proportional to the square of the number of resonators, when all the resonators are prepared in the same state. These superradiance properties can be used in life science research and clinical diagnostics dealing with small concentrations of analyte molecules, due to enhanced fluorescent properties of surface-bound molecules.

The physical mechanism of such collective emission and absorption effects is based on the interference of resonator decays, which plays an important part in other related effects, such as coupled resonator-induced transparency (CRIT) [170–173] and Bragg reflection of light from multiple quantum-well structures [174, 175]. The superradiance occurs when the individual cavity resonances are weakly coupled through waveguides or fibers under the condition, $L = 2\pi a$, where L is the path length between the resonators. In order to observe these effects in practical structures, the size uniformity of the cavities should be at the level of $\delta \sim 1/Q$, which in many cases exceeds the requirements for observation of tight-binding WG mode transport in overcoupled structures ($\delta \sim \kappa$). MRC technology can provide the required level of uniformity of cavities, thus opening the prospect for achieving superradiance properties in massive numbers of spheres with potential applications in ultrasensitive fluorescent sensors.

Due to high-Q factors of WG modes in spherical, cylindrical, or toroidal cavities, they are widely used in lab-on-chip and sensor applications [96–102]. In such microresonators, WG modes circulate thousands of times inside the cavity, which increases their interaction length with the nanoparticles, such as DNA, molecules, colloidal particles, or quantum dots, located in the vicinity of the resonators' surface. The conventional spectroscopic sensors [96–98, 100, 101] operate based on measurements of a spectral shift or broadening of corresponding WGM resonances. These studies have made it possible to develop sensors with extraordinarily high sensitivity, enabling single molecule detection [98]. Most recently, a new type of sensor device, based on the measurement of a fine splitting of WG mode peaks by the nanoparticles embedded in the cavity, has been proposed [99, 102]. In comparison with conventional spectroscopic sensors, such devices are less sensitive to the local heating effects and other environmental factors that give them a significant performance advantage in practical applications.

Clusters of microspheres have several important advantages over single spheres in sensor applications. Usually, a regime of weak coupling between WG modes in individual spheres is provided in such sensing clusters. It can be achieved either by separating cavities with resonant WG modes by a submicron gap [47, 95] or by assembling size-mismatched spheres [47, 48, 62, 64, 94] in a contact position. In weakly coupled clusters of identical spheres, the sensitivity of the molecule detection can be considerably enhanced, because a background-free detection can be implemented by either a spectral or spatial shift between the object and sensor

[95]. This allows achieving novel sensor functionalities, such as detection of the orientation of the dipole moment of the molecules attached to the spheres' surface [95], as illustrated in Fig. 17.17. On the other hand, the clusters formed by size-mismatched spheres usually display spectra containing very dense groups of WG mode peaks, due to contributions of all constituting cavities [62, 64, 94], as illustrated in Fig. 17.18b. Such spectra, compared to the single sphere emission spectra [94] in Fig. 17.18a, are more suitable for developing multi-wavelength sensors. In addition, clusters of microresonators offer the advantage of exhibiting specific WGM spectra, which can be considered as their fingerprint [94]. Therefore, individual clusters can be traced throughout an experiment even without the knowledge of their precise positions.

Besides sensor applications, arrays of size-mismatched microspheres can be used for developing compact high-resolution spectrometers [93]. The principle of operation of these devices has some similarity with multimodal-multiplex spectroscopy [176] in disordered photonic crystals, where wavelength-dependent patterns of scattered light have been used for identifying different wavelengths. However, the devices based on mesoscale ($a \geq \lambda$) spheres have better spectral resolution due to their high-Q WG mode resonances. The input light from a waveguide is resonantly coupled to such arrays of size-mismatched microspheres creating

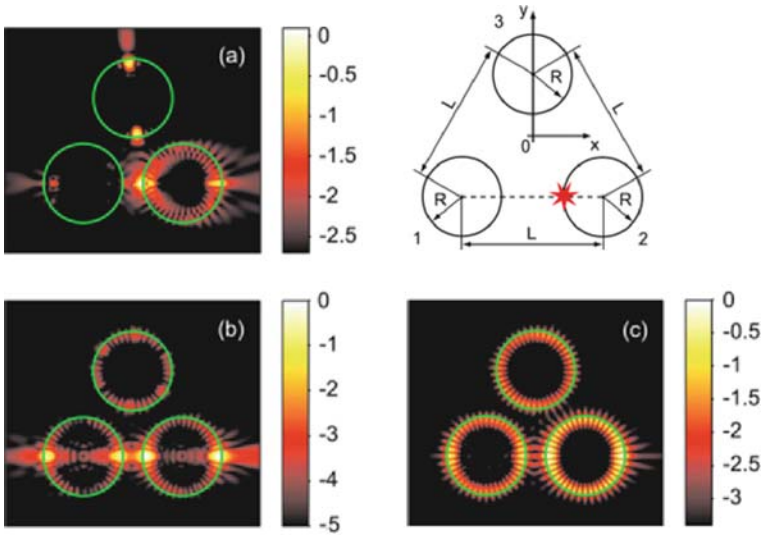

Fig. 17.17 Relative intensity distribution for the three-sphere ($a = R = 1.4\ \mu$m, $N = 1.59$) cluster calculated for $\lambda = 572$ nm. Orientation of the dipole moment is (**a**) along x-axis, (**b**) along y-axis, and (**c**) along z-axis. *Inset*: Layout of the sensing cluster of three identical weakly coupled spheres. The dipole source (*asterisk*) is located on a line connecting the centers of spheres 1 and 2. Sphere 3 is the sensing sphere and probes the dipole moment orientation [95]. Reprinted with permission. Copyright 2009 American Institute of Physics

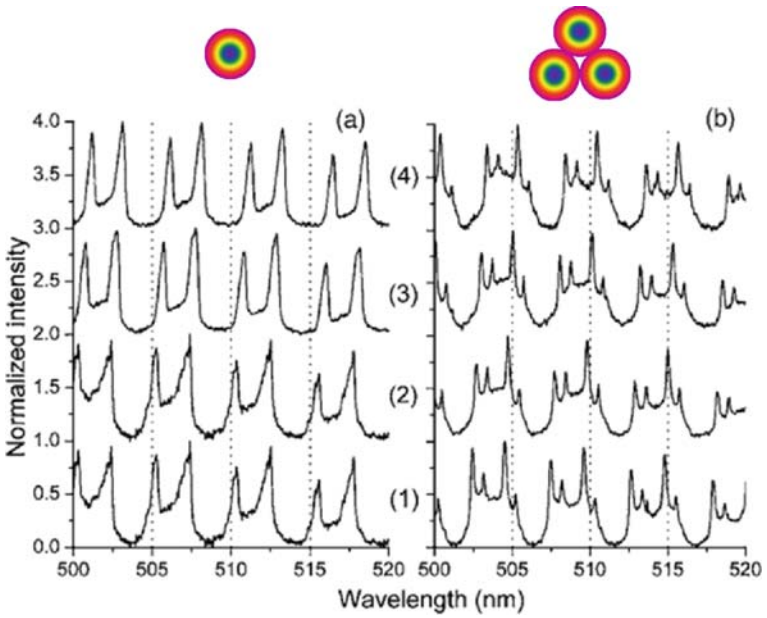

Fig. 17.18 WGM spectra of (**a**) a single microsphere ($a = 5\ \mu$m, $N = 1.59$) in an aqueous environment and (**b**) a cluster of three microspheres, respectively, upon sequential deposition of polymer layers [94]. Reprinted with permission. Copyright 2009 American Institute of Physics. Spectra 1–4 correspond to increasing thickness of the polymer layers

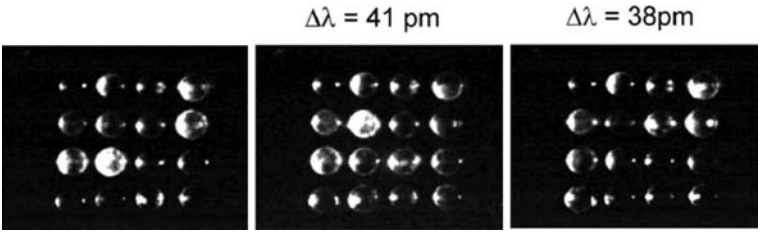

Fig. 17.19 Intensity distribution on the resonator array for three different wavelengths. From *left* to *right*: $\lambda = 685.3980$, 685.3569, 685.3189 nm [93]. Reprinted with permission. Copyright 2009 Optical Society of America

wavelength-dependent intensity distributions, as shown in Fig. 17.19. A wavelength resolution of $\lambda/\Delta\lambda = 7 \times 10^7$ has been demonstrated [93] for such devices.

Finally, the microspheres can be used for developing applications based on their nonresonant properties of focusing light. This area was stimulated by recent observations of photonic nanojets [86–92] and near-field effects in the focusing properties [150–154] of mesoscale spheres. In such photonic nanojects, the intensity of light in the middle of the focused spot exceeds the intensity of the illuminating wave by a factor of $\sim 10^3$. The focused spot has the full-width-half-maximum (FWHM) beamwidth between one-third and one-half of the wavelength in the background

medium and is only weakly dependent on the size of the dielectric sphere. The light waves propagate in the focal spot area with little divergence for several wavelengths. These properties have been used in several application areas, such as nanoparticle detection [87, 90], detection of subwavelength pits in the optical data-storage disks [92], locally enhanced Raman scattering [177], high-resolution Raman imaging [178], and subwavelength direct-write nanopatterning [179].

Large-area arrays of closely packed microspheres can be used for laser-induced periodical surface patterning [151]. In this case, the illumination is provided perpendicular to the plane of array, and the spheres behave as individual microlenses.

A particularly interesting case is represented by illumination along the long chains of microspheres, leading to the periodical focusing of light effects [57–60] described in Section 17.5.6. Propagation of light in such chains leads to the formation of photonic nanojets with progressively smaller sizes, which can be used for developing a variety of biomedical applications, including ultra-precise laser tissue surgery. The optical transport losses of such systems can, in principle, be reduced by assembling chains of spheres inside hollow waveguides. For a certain range of parameters of spheres and waveguide the resulting transmitted and reflected power has been analyzed [180] using a rigorous integral equation formulation.

17.7 Conclusions

The studies of different types of coupled cavities, microrings, disks, toroids, photonic crystal defects, and microspheres are based on common ideas of tight-binding of photonic atoms [3–7], critical coupling [181], impedance matching [182], Fano resonances [47, 146–148], optical supermodes [131], disorder-induced scattering [24], localization [25, 26], and percolation [64] of light. From an engineering perspective, some of these structures show great potential for use in device applications. Examples include ultracompact buffers on a silicon chip [23] and error-free continuously tunable delay lines at 10 Gbit/s based on silicon oxynitride microrings [168]. Along with already established devices, this area shows significant potential for discovering new physical effects and designing structures with unique functionality. Examples of this include novel structures harnessing optical forces in integrated photonic circuits [156–160], effects of collective emission and absorption [171], and effects of dynamical tuning of cavities [183].

The resonant optical properties of coupled cavities can be engineered on the basis of tight-binding WG modes in photonic atoms. In practice, however, this requires an independent tuning of the individual cavity resonances, which is a rather difficult problem in chip-scale structures. Microspheres, in this regard, are unique cavities since they can be pre-sorted with the size uniformity, $\delta \sim 1/Q$, which is not available for other types of cavities fabricated by the well-established lithographic and etching techniques. Small quantities of size-matched spheres can be sorted by spectroscopically controlled micromanipulation. Future development of MRC technology is likely to be connected with massively parallel sorting of spheres based on using size-selective radiative pressure [67, 68].

This extraordinarily high level of size uniformity allows the development of novel structures and devices with unique functionality. Due to controllable dispersions for photons, collective emission and absorption, and enhanced light–matter coupling, such structures can be used for developing coupled arrays of microlasers, ultracompact high-resolution spectrometers, and sensors. Cavities with high-Q WG modes are widely used in lab-on-chip and sensor applications [96–102] for detecting nanoparticles, such as DNA, molecules, colloidal particles, or quantum dots, located in the vicinity of the resonators' surface. Sensors based on clusters of microspheres with weakly coupled WG modes can significantly extend the functionality of single-cavity devices, adding such features as multi-wavelength [94] and background-free [95] detection.

Another unique property of mesoscale ($a \geq \lambda$) microspheres is connected with their ability to focus collimated beams into subwavelength spots termed nanoscale photonic nanojets [86–92]. This property has been used in a variety of applications [150–154, 177–179]. In linear chains of microspheres, such focusing effects can be periodically reproduced giving rise to novel NIMs [57–60] with small propagation losses and progressively smaller sizes of the focused spots along the chains. These focusing effects occur in a broad range of wavelengths in comparison with the resonant WG coupling effects. Integrated chains of microspheres can be used for developing novel optical scalpels and optical microprobes with subwavelength spatial resolution.

Acknowledgments The author would like to thank S.V. Boriskina, A.B. Matsko, M. Sumetsky, U. Woggon, A. Taflove, S. Arnold, A. Melloni, Y.A. Vlasov, M.S. Skolnick, J.J. Baumberg, and M.A. Fiddy for useful discussions. The author thanks M.D. Kerr and R. Hudgins for a critical reading of the manuscript and useful comments. This work was supported by the US Army Research Office (ARO) under grant No. W911NF-09-1-0450 (J.T. Prater), by the National Science Foundation (NSF) under grant ECCS-0824067, and, in part, by funds provided by The University of North Carolina at Charlotte.

References

1. Ashcroft, N.W., Mermin, N.D. Solid state Physics. Saunders (1976)
2. Kittel, C. Introduction to solid state Physics. John Wiley and Sons, New York, 7th ed. (1996)
3. De Sterke, C.M. Superstructure gratings in the tight-binding approximation. Phys. Rev. E **57**, 3502–3509 (1998)
4. Stefanou, N., Modinos, A. Impurity bands in photonic insulators. Phys. Rev. B **57**, 12127–12133 (1998)
5. Lidorikis, E., Sigalas, M.M., et al. Tight-binding parametrization for photonic band gap materials. Phys. Rev. Lett. **81**, 1405-1408 (1998)
6. Yariv, A., Xu, Y., et al. Coupled-resonator optical waveguide: A proposal and analysis. Opt. Lett. **24**, 711–713 (1999)
7. Bayindir, M., Temelkuran, B., et al. Tight-binding description of the coupled defect modes in three-dimensional photonic crystals. Phys. Rev. Lett. **84**, 2140–2143 (2000)
8. Little, B.E., Chu, S.T., et al. Microring resonator channel dropping filters. J. Lightw. Tehnnol. **15**, 998–1005 (1997)
9. Heebner, J.E., Boyd, R.W., et al. SCISSOR solitons and other novel propagation effects in microresonator-modified waveguides. J. Opt. Soc. Am. B **19**, 722–731 (2002)

10. Sumetsky, M., Eggleton, B.J. Modeling and optimization of complex photonic resonant cavity circuits. Opt. Express **11**, 381–391 (2003)
11. Smith, D.D., Chang, H., et al. Whispering-gallery mode splitting in coupled microresonators. J. Opt. Soc. Am. B **20**, 1967–1974 (2003)
12. Heebner, J.E., Chak, P., et al. Distributed and localized feedback in microresonator sequences for linear and nonlinear optics. J. Opt. Soc. Am. B **21**, 1818–1832 (2004)
13. Matsko, A.B., Savchenkov, A.A., et al. Interference effects in lossy resonator chains. J. Modern Opt. **51**, 2515–2522 (2004)
14. Deng, S., Cai, W., et al. Numerical study of light propagation via whispering gallery modes in microcylinder coupled resonator optical waveguides. Opt. Express **12**, 6468–6480 (2004)
15. Khurgin, J.B. Expanding the bandwidth of slow-light photonic devices based on coupled resonators. Opt. Lett. **30**, 513–515 (2005)
16. Boriskina, S.V., Benson, T.M., et al. Optical modes in 2-D imperfect square and triangular microcavities. IEEE J. Quant. Electron. **41**, 857–862 (2005)
17. Zhuk, V., Regelman, D.V., et al. Near-field mapping of the electromagnetic field in con-fined photon geometries. Phys. Rev. B **66**, 115302 (2002)
18. Oliver, S., Smith, C., et al. Miniband transmission in a photonic crystal coupled-resonator optical waveguide. Opt. Lett. **26**, 1019–1021 (2001)
19. Bristow, A.D., Whittaker, D.M., et al. Defect states and commensurability in dual-period AlxGa1-xAs photonic crystal waveguides. Phys. Rev. B **68**, 033303 (2003)
20. Guven, K., Ozbay, E. Coupling and phase analysis of cavity structures in two-dimensional photonic crystals. Phys. Rev. B **71**, 085108 (2005)
21. Little, B.E., Chu, S.T., et al. Very high-order microring resonator filters for WDM applications. IEEE Photon. Technol. Lett. **16**, 2263–2265 (2004)
22. Poon, J.K.S., Zhu, L., et al. Transmission and group delay of microring coupled-resonator optical waveguides. Opt. Lett. **31**, 456–458 (2006)
23. Xia, F., Sekaric, L., et al. Ultra-compact optical buffers on a silicon chip. Nat. Photon. **1**, 65–71 (2007)
24. Möller, B.M., Woggon, U., et al. Bloch modes and disorder phenomena in coupled resonator chains. Phys. Rev. B **75**, 245327 (2007)
25. Mookherjea, S., Park, J.S., et al. Localization in silicon nano-photonic slow-light waveguides. Nat. Photon. **2**, 90–93 (2008)
26. Fussell, D.P., Hughes, S., et al. Influence of fabrication disorder on the optical properties of coupled cavity photonic crystal waveguides. Phys. Rev. B **78**, 144201 (2008)
27. Choi, S.J., Peng, Z., et al. Tunable microdisk resonators vertically coupled to bus waveguides using epitaxial regrowth and wafer bonding techniques. Appl. Phys. Lett. **84**, 651–653 (2004)
28. Maune, B., Lawson, R., et al. Electrically tunable ring resonators incorporating nematic liquid crystals as cladding layers. Appl. Phys. Lett. **83**, 4689–4691 (2003)
29. Armani, D., Min, B., et al. Electrical thermo-optic tuning of ultra-high-Q microtoroid resonators. Appl. Phys. Lett. **85**, 5439–5441 (2004)
30. For a review see articles in Chang, R.K., Campillo, A.J. Optical Processes in Micro-cavities. World Scientific, Singapore (1996)
31. Benner, R.E., Barber, P.W., et al. Observation of structure resonances in the fluorescence spectra from microspheres. Phys. Rev. Lett. **44**, 475–478 (1980)
32. Gorodetsky, M.L., Savchenkov, A.A., et al. Ultimate Q of optical micro-sphere resonators. Opt. Lett. **21**, 453–455 (1996)
33. Vahala, K.J. Optical microcavities. Nature **424**, 839–846 (2003)
34. For a recent review see: Matsko, A.B., Ilchenko, V.S. Optical resonators with whispering gallery modes – part I: Basics. IEEE J. Sel. Top. Quant. Electron. **12**, 3–14 (2006)
35. For a recent review see: Ilchenko, V.S., Matsko, A.B. Optical resonators with whispering-gallery modes – part II: Applications. IEEE J. Sel. Top. Quant. Electron. **12**, 15–32 (2006)

36. http://www.thermofisher.com/global/en/home.asp. Assessed 22 August 2009.
37. http://www.bangslabs.com/products/nist_traceable_particle_size_standards. Assessed 22 August 2009.
38. http://www.polysciences.com/. Assessed 22 August 2009.
39. http://www.microspheres-nanospheres.com/. Assessed 22 August 2009.
40. Serpengüzel, A., Kurt, A., et al. Silicon microspheres for electronic and photonic integration. Photonics and Nanostructures – Fundamentals and Applications **6**, 179–182 (2008)
41. Fuller, K.A. Optical resonances and two-sphere systems. Appl. Optics **30**, 4716 (1991)
42. Mukaiyama, T., Takeda, K., et al. Tight-binding photonic molecule modes of resonant biospheres. Phys. Rev. Lett. **82**, 4623–4626 (1999)
43. Miyazaki, H., Jimba, Y. Ab initio tight-binding description of morphology-dependent resonance in a biosphere. Phys. Rev. B **62**, 7976–7997 (2000)
44. Hara Y., Mukaiyama, T., et al. Photonic molecule lasing. Opt. Lett. **28**, 2437–2439 (2003)
45. Möller, B.M., Woggon, U., et al. Photonic molecules doped with semiconductor nanocrystals. Phys. Rev. B **70**, 115323 (2004)
46. Rakovich, Y.P., Donegan, J.F., et al. Fine structure of coupled optical modes in photonic molecules. Phys. Rev. A **70**, 051801 (2004)
47. Kanaev, A.V., Astratov, V.N., et al. Optical coupling at a distance between detuned spherical cavities. Appl. Phys. Lett. **88**, 111111 (2006)
48. Ashili, S.P., Astratov, V.N., et al. The effects of inter-cavity separation on optical coupling in dielectric biospheres. Opt. Express **14**, 9460–9466 (2006)
49. Deych, L.I., Schmidt, C., et al. Optical coupling of fundamental whispering-gallery modes in bispheres. Phys. Rev. A **77**, 051801(R) (2008)
50. Barnes, M.D., Mahurin, S.M., et al. Three-dimensional photonic "molecules" from sequentially attached polymer-blend microparticles. Phys. Rev. Lett. **88**, 015508 (2002)
51. Furukawa, H., Tenjimbayashi, K. Light propagation in periodic microcavities. Appl. Phys. Lett. **80**, 192–194 (2002)
52. Astratov, V.N., Franchak, J.P., et al. Optical coupling and transport phenomena in chains of spherical dielectric microresonators with size disorder. Appl. Phys. Lett. **85**, 5508–5510 (2004)
53. Hara, Y., Mukaiyama, T., et al. Heavy photon states in photonic chains of resonantly coupled cavities with supermonodispersive microspheres. Phys. Rev. Lett. **94**, 203905 (2005)
54. Möller, B.M., Woggon, U., et al. Coupled-resonator optical waveguides doped with nanocrystals. Opt. Lett. **30**, 2116–2118 (2005)
55. Chen, Z., Taflove, A., et al. Highly efficient optical coupling and transport phenomena in chains of dielectric microspheres. Opt. Lett. **31**, 389–391 (2006)
56. Deych, L.I., Roslyak, O. Photonic band mixing in linear chains of optically coupled microspheres. Phys. Rev. E **73**, 036606 (2006)
57. Kapitonov, A.M., Astratov, V.N. Observation of nanojet-inducing modes with small propagation losses in chains of coupled spherical cavities. Opt. Lett. **32**, 409–411 (2007)
58. Yang, S., Astratov, V.N. Photonic nanojet-induced modes in chains of size-disordered microspheres with an attenuation of only 0.08dB per sphere. Appl. Phys. Lett. **92**, 261111 (2008)
59. Mitsui, T., Wakayama, Y., et al. Light propagation within colloidal crystal wire fabricated by a dewetting process. Nano Lett. **8**, 853–858 (2008)
60. Mitsui, T., Wakayama, Y., et al. Observation of light propagation across a 900 corner in chains of microspheres on a patterned substrate. Opt. Lett. **33**, 1189–1191 (2008)
61. Kondo, T., Hangyo, M., et al. Transmission characteristics of a two-dimensional photonic crystal array of dielectric spheres us-ing subterahertz time domain spectroscopy. Phys. Rev. B **66**, 033111 (2002)
62. Gerlach, M., Rakovich, Y.P., et al. Nanojets and directional emission in sym-metric photonic molecules. Opt. Express **15**, 17343–17350 (2007)

63. Guo, H., Chen, H., et al. Transmission modulation in the passband of polystyrene photonic crystals. Appl. Phys. Lett. **82**, 373–375 (2003)
64. Astratov, V.N., Ashili, S.P. Percolation of light through whispering gallery modes in 3D lattices of coupled microspheres. Opt. Express **15**, 17351–17361 (2007)
65. Yang, S., Astratov, V.N. Spectroscopy of coherently coupled whispering-gallery modes in size-matched bispheres assembled on a substrate. Opt. Lett. **34**, 2057–2059 (2009)
66. Yang, S., Astratov, V.N. Spectroscopy of photonic molecular states in supermonodispersive biospheres. Published in Laser Resonators and Beam Control XI. In: Ku-dryashov, A.V., Paxton, A.H., Ilchenko, V.S., Aschke, L. Proc. of SPIE, Vol. 7194, paper 719411-1, Photonics West 2009, San Jose, January 24–29, 9 pp.
67. Ng, J., Chan, C.T. Size-selective optical forces for microspheres using evanescent wave excitation of whispering gallery modes. Appl. Phys. Lett. **92**, 251109 (2008)
68. Xiao, J.J., Ng, J., et al. Whispering gallery mode enhanced optical force with resonant tunneling excitation in the Kretschmann geometry. Appl. Phys. Lett. **94**, 011102 (2009)
69. Vyawahare, S., Craig, K.M., et al. Patterning lines by capillary flows. Nano Lett. **6**, 271–276 (2006)
70. Suh, K.Y. Surface-tension-driven patterning: combining tailored physical self-organization with microfabrication methods. Small **2**, 832–834 (2006)
71. Yin, Y., Lu, Y., et al. Template-assisted self-assembly: a practical route to complex aggregates of monodispersed colloids with well-defined sizes, shapes, and structures. J. Am. Chem. Soc. **123**, 8718–9729 (2001)
72. Ozin, G.A., Yang, S.M. The race for the photonic chip: colloidal crystal assembly in silicon wafers. Adv. Funct. Mater. **11**, 95–104 (2001)
73. Gates, B., Qin, D., et al. Assembly of nanoparticles into opaline structures over large areas. Adv. Mater. **11**, 466–469 (1999)
74. Curtis, J.E., Koss, B.A., et al. Dynamic holographic optical tweezers. Opt. Comm. **207**, 169–175 (2002)
75. Sinclair, G., Jordan, P., et al. Assembly of 3-dimensional structures using programmable holographic optical tweezers. Opt. Express **12**, 5475–5480 (2004)
76. Roichman, Y., Grier, D.G. Holographic assembly of quasicrystalline photonic heterostructures, Opt. Express **13**, 5434–5439 (2005)
77. White, G., Gibson, G., et al. An optical trapped microhand for manipulating micron-sized objects. Opt. Express **14**, 12497–12502 (2006)
78. Erenso, D., Shulman, A., et al. Formation of synthetic structures with micron size silica beads using optical tweezers. J. Mod. Opt. **207**, 169–175 (2002)
79. Benito, D.C., Carberry, D.M., et al. Constructing 3D crystal templates for photonic band gap materials using holographic optical tweezers. Opt. Express **16**, 13005–13015 (2008)
80. Chiou, P.Y., Ohta, A.T., et al. Massively parallel manipulation of single cells and microparticles using optical images. Nature **436**, 370–372 (2005)
81. Garcia-Santamaria, F., Miyazaki, H.T., et al. Nanorobotic manipulation of microspheres for on-chip diamond architectures. Adv. Mater. **14**, 1144–1147 (2002)
82. Lorenz, C.D., Ziff, R.M. Precise determination of the bond percolation thresholds in finite-size scaling corrections for the sc, fcc, and bcc lattices. Phys. Rev. E **57**, 230–236 (1998)
83. For a review on complex networks see: Albert, R., Barabasi, A.-L. Statistical mechanics of complex networks. Rev. Mod. Phys. **74**, 47–97 (2002)
84. Burlak, G., Diaz-de-Anda, A., et al. Critical behavior of nanoemitter radiation in a percolation material. Phys. Lett. A **373**, 1492–1499 (2009)
85. Burlak, G., Vlasova, M., et al. Optical percolation in ceramics assisted by porous clusters. Opt. Comm. **282**, 2850–2856 (2009)
86. Chen, Z., Taflove, A., et al. Photonic nanojet enhancement of backscattering of light by nanoparticles: a potential novel visible-light ultramicroscopy technique. Opt. Express **12**, 1214–1220 (2004).
87. Li, X., Chen, Z., et al. Optical analysis of nanoparticles via enhanced backscattering facilitated by 3-D photonic nanojets. Opt. Express **13**, 526–533 (2005)

88. Lecler, S., Takakura, Y., et al. Properties of a three-dimensional photonic jet. Opt. Lett. **30**, 2641–2643 (2005)
89. Itagi, A.V., Challener, W.A. Optics of photonic nanojets. J. Opt. Soc. Am. A **22**, 2847–2858 (2005)
90. Heifetz, A., Huang, K., et al. Experimental confirmation of backscattering enhancement induced by a photonic jet. Appl. Phys. Lett. **89**, 221118 (2006).
91. Ferrand, P., Wenger, J., et al. Direct imaging of photonic nanojets. Opt. Express **16**, 6930–6940 (2008)
92. Kong, S.-C., Sahakian, A., et al. Photonic nanojet-enabled optical data storage, Opt. Express **16**, 13713–13719 (2008)
93. Schweiger, G., Nett, R., et al. Microresonator array for high-resolution spectroscopy. Opt. Lett. **32**, 2644–2646 (2007)
94. Francois, A., Himmelhaus, M. Optical biosensor based on whispering gallery mode excitations in clusters of microparticles. Appl. Phys. Lett. **92**, 141107 (2008)
95. Guzatov, D.V., Woggon, U. Coupled microsphere clusters for detecting molecule's dipole moment orientation. Appl. Phys. Lett. **94**, 241104 (2009)
96. Vollmer, F., Braun, D., et al. Protein detection by optical shift of a resonant microcavity. Appl. Phys. Lett. **80**, 4057–4059 (2002)
97. Teraoka, I., Arnold, S. Theory of resonance shifts in TE and TM whispering gallery modes by nonradial perturbations for sensing applications. J. Opt. Soc. Am. B **23**, 1381–1389 (2006)
98. Armani, A.M., Kulkarni, R.P., et al. Label-free, single-molecule detection with optical microcavities. Science **317**, 783–787 (2007)
99. Hiremath, K.R., Astratov, V.N. Perturbations of whispering gallery modes by nanoparticles embedded in microcavities. Opt. Express **16**, 5421–5426 (2008)
100. Lutti, J., Langbein, W., et al. A monolithic optical sensor based on whispering-gallery modes in polystyrene microspheres. Appl. Phys. Lett. **93**, 151103 (2008)
101. Pang, S., Beckham, R.E., et al. Quantum dot-embedded microspheres for remote refractive index sensing. Appl. Phys. Lett. **92**, 221108 (2008)
102. Teraoka, I., Arnold, S. Resonance shifts of counterpropagating whispering-gallery modes: degenerate perturbation theory and application to resonator sensors with axial symmetry. J. Opt. Soc. of Am. B **26**, 1321–1329 (2009)
103. Astratov, V.N. Fundamentals and applications of microsphere resonator circuits. Proceedings of 11th International Conference on Transparent Optical Networks, Azores, June 28-July 2, 1–4 (2009)
104. Le Thomas, N., Woggon, U., et al. Effect of a dielectric substrate on whispering-gallery-mode sensors. J. Opt. Soc. Am. B **23**, 2361–2365 (2006)
105. Buck, J.R., Kimble, H.J. Optimal sizes of dielectric microspheres for cavity QED with strong coupling. Phys. Rev. A **67**, 033806 (2003)
106. Chang, R.K., Campillo, A.J. Optical processes in microcavities. World Scientific, Singapore (1996)
107. van de Hulst, H.C. Light scattering by small particles. Wiley, New York (1981)
108. Lam, C.C., Leung, P.T., et al. Explicit asymptotic formulas for the positions, widths, and strengths of resonances in Mie scattering. J. Opt. Soc. Am. B **9**, 1585–1592 (1992)
109. Arnaud, C., Boustimi, M., et al. Wavelength shifts in erbium doped glass micro-spherical whispering gallery mode lasers. Proceedings of the International Workshop on Photonics and Applications, Hanoi, Vietnam, 209–220 (2004)
110. Braginsky, V.B., Gorodetsky, M.L., et al. Quality-factor and nonlinear properties of optical whispering gallery modes. Phys. Lett. A **137**, 393–397 (1989)
111. Ilchenko V.S., Volkov P.S., et al. Strain-tunable high-Q optical microsphere resonator. Opt. Comm. **145**, 86–90 (1998)
112. Gerlach, M., Rakovich, Y.P., et al. Radiation-pressure-induced mode splitting in a spherical microcavity with an elastic shell. Opt. Express **15**, 3597–3606 (2007)

113. Quake, S.R., Scherer, A. From micro- to nanofabrication with soft materials. Science **290**, 1536–1540 (2000)
114. Psaltis, D., Quake, S.R., et al. Developing optofluidic technology through the fusion of microfluidic and optics. Nature **442**, 381–386 (2006)
115. Astratov, V.N., Bogomolov, V.N., et al. Optical spectroscopy of opal matrices with CdS embedded in its pores: quantum confinement and photonic band gap effects. Nuovo Cimento D **17**, 1349–1354 (1995)
116. Astratov, V.N., Vlasov, Y.A., et al. Photonic band gaps in 3D ordered FCC silica matrices. Phys. Lett. A **222**, 349–353 (1996)
117. Vlasov, Y.A., Astratov, V.N., et al. Manifestation of intrinsic defects in the optical properties of self-organized opal photonic crystals. Phys. Rev. E **61**, 5784–5793 (2000)
118. Astratov, V.N., Adawi, A.M., et al. Interplay of order and disorder in the optical properties of opal photonic crystals. Phys. Rev. B **66**, 165215 (2002)
119. Denkov, N., Velev, O., et al. Two-dimensional crystallization. Nature (London) **361**, 26 (1993)
120. Bertone, J.F., Jiang, P., et al. Thickness dependence of the optical properties of ordered silica-air and air-polymer photonic crystals. Phys. Rev. Lett. **83**, 300–303 (1999)
121. van Blaaderen, A., Ruel, R., et al. Template-directed colloidal crystallization, Nature (London) **385**, 321–324 (1997)
122. Lin, K.-h., Crocker, J.C., et al. Entropically driven colloidal crystallization on patterned substrates. Phys. Rev. Lett. **85**, 1770–1773 (2000)
123. Yang, S.M., Miguez, H., et al. Opal circuits of light – planarized micophotonic crystal chips. Adv. Funct. Mater. **12**, 425–431 (2002)
124. Möller, B.M., Artemyev, M.V., et al. Bloch modes and group velocity delay in coupled resonator chains. Phys. Stat. Sol. (a) **204**, 3636–3646 (2007)
125. Ashkin, A., Dziedzic, J.M., et al. Observation of a single-beam gradient force optical trap for dielectric particles. Opt. Lett. **11**, 288–290 (1986)
126. Grier, D.G. A revolution in optical manipulation. Nature **124**, 810–816 (2003)
127. Curtis, J.E., Koss, B.A., et al. Dynamic holographic optical tweezers. Opt. Commun. **207**, 169–175 (2002)
128. Armitage, A., Skolnick, M.S., et al. Optically induced splitting of bright excitonic states in coupled quantum microcavities. Phys. Rev. B. **57**, 14877–14881 (1998)
129. Atlasov, K.A., Karlsson, K.F., et al. Wavelength and loss splitting in directly coupled photonic-crystal defect microcavities. Opt. Express **16**, 16255–16264 (2008)
130. Ryu, J.-W., Lee, S.-Y., et al. Directional interacting whispering-gallery modes in coupled dielectric microdisks. Phys. Rev. A **74**, 013804 (2006)
131. Boriskina, S.V. Theoretical prediction of a dramatic Q-factor enhancement and de-generacy removal of whispering gallery modes in symmetrical photonic molecules. Opt. Lett. **31**, 338–340 (2006)
132. Chremmos, I., Uzunoglu, N. Modes of the infinite square lattice of coupled microring resonators. J. Opt. Soc. Am. A **25**, 3043–3050 (2008)
133. Schwefel, H.G.L., Poulton, C.G. An improved method for calculating resonances of multiple dielectric disks arbitrarily positioned in the plane. Opt. Express **17**, 13178–13186 (2009)
134. Yang, S. Ph.D. thesis entitled "Spectroscopic study of optical confinement and transport effects in coupled microspheres and pillar cavities." University of North Carolina at Charlotte (2009)
135. Spreeuw, R.J.C., Beijersbergen, M.W., et al. Optical ring cavities as tailored four-level systems: An application of the group U (2,2). Phys. Rev. A **45**, 1213–1229 (1992)
136. Kavokin, A.V., Baumberg, J.J., et al. Microcavities. Oxford University Press Inc., New York (2007)
137. Weisbuch, C., Nishioka, M., et al. Observation of coupled exciton–photon mode splitting in a semiconductor quantum microcavity. Phys. Rev. Lett. **69**, 3314–3317 (1992)

138. Whittaker, D.M., Kinsler, P., et al. Motional narrowing in semiconductor microcavities. Phys. Rev. Lett. **77**, 4792–4795 (1996)
139. Sermage, B., Long, S., et al. Time-resolved spontaneous emission of excitons in a microcavity: Behavior of the individual exciton-photon mixed states. Phys. Rev. B **53**, 16516–16523 (1996)
140. Heiss, W.D. Repulsion of resonance states and exceptional points. Phys. Rev. E **61**, 929–932 (2000)
141. Wiersig, J. Formation of long-lived, scarlike modes near avoided resonance crossings in optical microcavities. Phys. Rev. Lett. **97**, 253901 (2006)
142. Boriskina, S.V. Coupling of whispering-gallery modes in size mismatched microdisk photonic molecules. Opt. Lett. **32**, 1557–1559 (2007)
143. Ryu, J.-W., Lee, S.-Y., et al. Coupled nonidentical microdisks: Avoided crossing of energy levels and unidirectional far-field emission. Phys. Rev. A **79**, 053858 (2009)
144. Nakagawa, A., Ishii, S., et al. Photonic molecule laser composed of GaInAsP microdisks. Appl. Phys. Lett. **86**, 041112 (2005)
145. Benyoucef, M., Kiravittaya, S., et al. Strongly cou-pled semiconductor microcavities: A route to couple artificial atoms over micrometric distances. Phys. Rev. B **77**, 035108 (2008)
146. Fano, U. Effects of configuration interaction on intensities and phase shifts. Phys. Rev. **124**, 1866–1878 (1961)
147. Astratov, V.N., Whittaker, D.M., et al. Photonic Band Structure Effects in the Reflectivity of Periodically Patterned Waveguides. Phys. Rev. B **60**, R16255–R16258 (1999)
148. Fan, S. Sharp asymmetric line shapes in side-coupled waveguide-cavity systems. Appl. Phys. Lett. **80**, 908–910 (2002)
149. Hecht, E. Optics (4th ed.). Pearson Education, Inc., San Francisco, CA, USA (2002).
150. Mosbacher, M., Münzer, H.-J., et al. Optical field enhancement effects in laser-assisted particle removal. Appl. Phys. A: Mater. Sci. Process. **72**, 41–44 (2001)
151. Piglmayer, K., Denk, R., et al. Laser-induced surface patterning by means of microspheres. Appl. Phys. Lett. **80**, 4693–4695 (2002)
152. Luk'yanchuk, B.S., Arnold, N., et al. Three-dimensional effects in dry laser cleaning. Appl. Phys. A: Mater. Sci. Process. **77**, 209–215 (2003)
153. Luk'yanchuk, B.S., Wang, Z.B., et al. Particle on surface: 3D-effects in dry laser cleaning. Appl. Phys. A: Mater. Sci. Process. **79**, 747–751 (2004)
154. Zhou, Y., Hong, M.H., et al. Direct femtosecond laser nanopatterning of glass substrate by particle-assisted near-field enhancement. Appl. Phys. Lett. **88**, 023110 (2006)
155. Ferrari, C., Morichetti, F., et al. Disorder in coupled-resonator optical wave-guides. J. Opt. Soc. Am. B **26**, 858–866 (2009)
156. Kippenberg, T.J., Vahala, K.J. Cavity opto-mechanics, Opt. Express **15**, 17172–17205 (2007)
157. Li, M., Pernice, W.H.P., et al. Harnessing optical forces in integrated photonic circuits. Nature **456**, 480–484 (2008)
158. Camacho, R.M., Chan, J., et al. Characterization of radiation pressure and thermal effects in a nanoscale optomechanical cavity. Opt. Express **17**, 15726–15735 (2009)
159. Mellor, C.D., Bain, C.D. Array formation in evanescent waves. ChemPhysChem **7**, 329–332 (2006).
160. Povinelli, M.L., Johnson, S.G., et al. High-Q enhancement of attractive and repulsive optical forces between coupled whispering gallery-mode resonators. Opt. Express **13**, 8286–8295 (2005)
161. Ishii, S., Baba, T. Bistable lasing in twin microdisk photonic molecules. Appl. Phys. Lett. **87**, 181102 (2005)
162. Altug, H., Vuckovic, J. Photonic crystal nanocavity array laser. Opt. Express. **13**, 8819–8828 (2005)
163. Gourley, P.L, Warren, M.E., et al. Coherent beams from high efficiency two-dimensional surface-emitting semiconductor laser arrays. Appl. Phys. Lett. **58**, 890–892 (1991).

164. Serkland, D.K., Choquette, K.D., et al. Two-element phased array of antiguided vertical-cavity lasers. Appl. Phys. Lett. **75**, 3754–3756 (1999)
165. Raftery, J.J., Jr., Lehman, A.C., et al. In-phase evanescent coupling of two-dimensional arrays of defect cavities in photonic crystal vertical cavity surface emitting lasers. Appl. Phys. Lett. **89**, 081119 (2006)
166. Schwelb, O. Band-Limited optical mirrors based on ring resonators: Analysis and design. J. Lightw. Technol. **23**, 3931–3946 (2005)
167. Chremmos, I., Schwelb, O. Optimization, bandwidth and the effect of loss on the characteristics of the coupled ring reflector. Opt. Comm. **282** 3712–3719 (2009)
168. Morichetti, F., Melloni, A., et al. Error-free continuously-tunable delay at 10 Gbit/s in a reconfigurable on-chip delay-line. Opt. Express **16**, 8395–8405 (2008)
169. Matsko, A.B., Savchenkov, A.A., et al. Collective emission and absorption in a linear resonator chain. Opt. Express **17**,15210–15215 (2009)
170. Smith, D.D., Chang, H., et al. Coupled-resonator-induced transparency. Phys. Rev. A **69**, 063804 (2004)
171. Matsko, A.B., Savchenkov, A.A., et al. Interference effects in lossy resonator chains. J. Mod. Opt. **51**, 2515–2522 (2004)
172. Naweed, A., Farca, G., et al. Induced transparency and absorption in coupled whispering-gallery microresonators. Phys. Rev. A **71**, 043804 (2005)
173. Xu, Q., Sandhu, S., et al. Experimental realization of an on-chip all-optical analogue to electromagnetically induced transparency. Phys. Rev. Lett. **96**, 129901 (2006)
174. Ivchenko, E.L., Nesvizhskii, A.I., et al. Bragg reflection of light from quantum-well structures. Phys. Solid State **36**, 1156–1161 (1994).
175. Hubner, M., Prineas, J.P., et al. Optical lattices achieved by excitons in periodic quantum well structures. Phys. Rev. Lett. **83**, 2841–2844 (1999)
176. Xu, Z.C., Wang, Z.L., et al. Multimodal multiplex spectroscopy using photonic crystals. Opt. Express **11**, 2126–2133 (2004)
177. Yi, K.J., Wang, H., et al. Enhanced Raman scattering by self-assembled silica spherical microparticles. J. Appl. Phys. **101**, 063528 (2007)
178. Kasim, J., Ting, Y., et al. Near-field Raman imaging using optically trapped dielectric microsphere. Opt. Express **16**, 7976–7984 (2008)
179. McLeod, E., Arnold, C.B. Subwavelength direct-write nanopatterning using optically trapped microspheres. Nature Nanotech. **3**, 413–417 (2008)
180. Chremmos, I., Uzunoglu, N.K. Analysis of scattering by a linear chain of spherical inclusions in an optical fiber. J. Opt. Soc. Am. A **23**, 3054–3062 (2006)
181. Cai, M., Painter, O., et al. Observation of critical coupling in a fiber taper to a silica-microsphere whispering-gallery mode system, Phys. Rev. Lett. **85**, 74–76 (2000)
182. Di Falco, A., Conti, C., et al. Impedance matching in photonic crystal micro-cavities for second-harmonic generation. Opt. Lett. **31**, 250–253 (2006)
183. Preble, S., Xu, Q., et al. Changing the colour of light in a silicon resonator, Nat. Photon. **1**, 293–296 (2007)